nature immunology

Resource

https://doi.org/10.1038/s41590-025-02218-3

Mammary intraepithelial lymphocytes and intestinal inputs shape T cell dynamics in lactogenesis

Received: 25 June 2024

Accepted: 12 June 2025

Published online: 29 July 2025

Check for updates

Abigail Jaquish[1,2], Eleni Phung[1], Xutong Gong[3], Pilar Baldominos[4], Silvia Galván-Peña[3], Ian Magill[3], Isabelle Bursulaya[1], Eleonora Marina[4], ImmgenT consortium*, Kerri Bertrand[5], Christina Chambers[5], Andrés R. Muñoz-Rojas[6], Judith Agudo[3,5,7,8], Diane Mathis[3], Christophe Benoist[3] & Deepshika Ramanan[1,3]

Pregnancy brings about profound changes in the mammary gland to prepare for lactation, yet immunocyte changes that accompany this rapid remodeling are incompletely understood. We comprehensively analyzed mammary T cells, revealing a marked increase in $CD4^+$ and $CD8^+$ T effector cells, including an expansion of T cell receptor (TCR)$\alpha\beta^+CD8\alpha\alpha^+$ cells, in pregnancy and lactation. T cells were localized in the mammary epithelium, resembling intraepithelial lymphocytes (IELs) typically found in mucosal tissues. Similarity to mucosal tissues was substantiated by demonstrating partial dependence on microbial cues, T cell migration from the intestine to the mammary gland in late pregnancy and shared TCR clonotypes between intestinal and mammary tissues, including intriguing public TCR families. Putative counterparts of mammary IELs were found in human breast and milk. Mammary IELs are thus poised to manage the transition from a nonmucosal tissue to a mucosal barrier during lactogenesis.

The mammary gland is remarkable in its capacity to undergo multiple cycles of growth and regression during reproductive years. Mammary gland remodeling is largely driven by hormonal cues that guide stage specific adaptations during puberty, pregnancy, lactation and involution[1–3]. Pregnancy initiates mammary epithelial cell proliferation and ductal branching to support lactogenesis, a crucial process that ensures the production and transfer of breast milk, essential for offspring health[4,5]. The transition of the mammary gland into a secretory organ during lactation involves dramatic restructuring of cell composition and tissue enlargement, and increased exposure to the outside environment, including microbes on the maternal skin and offspring's oral cavity, rendering it a temporary barrier tissue[6,7]. The end of lactation triggers mammary involution, a reversal to its nonsecretory state marked by extensive apoptosis and tissue shrinkage[8,9]. The physiological stress that accompanies the rapid transformation of the mammary gland requires an extensive support network, including immunocytes, but the types of immunocytes involved and their functions in lactogenesis are unclear.

Innate and adaptive immunocytes are involved in immune regulation of the mammary gland at various developmental stages. Mast cells and eosinophils promote ductal branching during mammary gland development in puberty[10,11]. Macrophages are required for mammary

[1]NOMIS Center for Immunobiology and Microbial Pathogenesis, Salk Institute for Biological Studies, La Jolla, CA, USA. [2]Biological Sciences Graduate Program, University of California, San Diego, La Jolla, CA, USA. [3]Department of Immunology, Harvard Medical School, Boston, MA, USA. [4]Department of Cancer Immunology and Virology, Dana-Farber Cancer Institute, Boston, MA, USA. [5]Department of Pediatrics, University of California, San Diego, La Jolla, CA, USA. [6]Department of Biomedical Engineering, Rensselaer Polytechnic Institute, Troy, NY, USA. [7]Parker Institute for Cancer Immunotherapy at Dana-Farber Cancer Institute, Boston, MA, USA. [8]New York Stem Cell Foundation, New York, NY, USA. *A list of authors and their affiliations appears at the end of the paper. e-mail: dramanan@salk.edu

gland morphogenesis in puberty, alveologenesis in pregnancy and tissue regression in involution[11–16]. Specialized macrophage populations, such as ductal macrophages and lactation-induced macrophages (liMacs) support lactogenesis and milk production[12,17]. B cells, specifically IgA- and IgG-producing plasma cells, are abundant in lactation and promote offspring health by shaping the antibody composition of milk. We and others have shown that IgA-producing plasma cells can migrate from the intestine to the mammary gland in a CCL28 dependent manner[18–22]. Despite recent advances, our comprehension of various immunocyte types and their collaborative roles in facilitating mammary remodeling and regulating milk composition remains limited.

T cells maintain tissue homeostasis by promoting defense, tolerance, tissue repair and regulating cellular turnover. In the mammary gland, $CD4^+$ T cells have been described in puberty, and a subset of $CD4^+$ regulatory T (T_{reg}) cells that express RORγ increase during involution[23,24]. In addition, $CD4^+$ and $CD8^+$ T cells are present in milk[25]. Mammary $\gamma\delta^+$ T cells with innate-like properties increase during lactation and may protect against mammary oncogenesis[26]. Lactogenesis involves epithelial cell stress from rapid expansion and milk production and heightened exposure to the sudden increase in newly revealed self-antigens, which could create a conundrum for T cell tolerance. Yet, there is a large gap in our understanding of which T cell subsets are involved in lactogenesis and how they contribute to tissue specific adaptations in the mammary gland.

We set out to define immunocyte changes in lactogenesis and uncovered new T cell dynamics in the mammary gland. We provide a detailed overview of mammary intraepithelial T cells, shaped by intestinal and microbial influences, that accompany the remodeling of the mammary gland into a mucosal-like state during lactogenesis.

Results

Lactation leads to increased T cells in the mammary gland

The size and composition of the mammary gland undergo substantial changes in preparation for lactation, yet there remains a gap in our understanding of how immunocytes adapt to, and perhaps facilitate, those transitions. We quantified mammary immunocytes ($CD45^+$) across developmental stages by flow cytometry and found that gestation initiated a rapid increase in the total number of immunocytes, which was maintained in lactation and involution (Fig. 1a). To determine the expanding cell types and chart their adaptations, we performed a temporal analysis of immunocytes across different stages in female C57BL/6 (B6) mice; profiling by single-cell RNA sequencing (scRNA-seq) mammary glands from nulliparous, gestation (day 17), early lactation (day 3 postpartum) and involution (day 1 post-weaning) stages. A total of 60,060 immunocytes were captured across all lineages from 20 mice across three independent runs, revealing increased representation of T cell populations (Fig. 1a,b). Validation by flow cytometry confirmed the expansion of T cells, while the proportion of myeloid cells, which dominated in the nulliparous, declined somewhat (while remaining the largest cell populations, as previously described[12,17,24]) (Fig. 1b). Analysis of the scRNA-seq data revealed several myeloid cell populations, including the recently described lactation-associated liMacs, specifically during lactation[17] (Extended Data Fig. 1b,c). While we did not observe shifts in B cell populations (excluding plasma B cells), we identified $CD103^+$ natural killer (NK) cells that were associated with lactation (Extended Data Fig. 1a,d). To better understand the expanding T cell populations, we applied Louvain clustering[27], which parsed six clusters of T cells, which were annotated as naive T (T_n) cells and effector T (T_{eff}) cells that were either $CD4^+$, $CD8\alpha\beta^+$ or $CD8\alpha^+CD8\beta^-$ (CD8αα), and $CD4^-CD8^-CD3^+$ (double negative; DN) (Fig. 1c and replicate in Extended Data Fig. 2a) (gene signatures from ImmGen[28–30]). There was a shift in T cell receptor (TCR)β^+ populations, from mostly naive T cells before and during gestation to mostly activated states during lactation, with a particularly striking increase in $TCR\beta^+CD8\alpha\alpha^+$ cells in late pregnancy that persisted during involution (Fig. 1c,d), which we confirmed by flow cytometry (Extended Data Fig. 2b).

In contrast to the $CD8\alpha\beta^+$ T_{eff} cells characterized by *Itgb1* and *Cxcr6* expression, $CD8\alpha\alpha^+$ T cells expressed high levels of *Klrb1c*, *Cd160*, *Itgae* and *Gzmb*, suggesting increased cytotoxic potential and tissue residency (Fig. 1e and Extended Data Fig. 3a). $CD8\alpha\alpha^+$ T cells also expressed increased cell adhesion and proliferation genes such as *Mcm5*, *Mcm7*, *Mki67*, *Lgals1* and *Hmmr* in differential levels across stages (Extended Data Figs. 2c,d and 3a). The transcriptional signature of mammary $TCR\beta^+CD8\alpha\alpha^+$ cells was reminiscent of $CD8\alpha\alpha^+$ T cells[28,30] that have innate properties and reside in the epithelium of mucosal tissues, referred to as intraepithelial lymphocytes (IELs) (intestinal $CD8\alpha\alpha^+$ IEL signature[30,31] applied to mammary $CD8\alpha\alpha^+$ cluster in Fig. 1d). A similar signature has also been described in $TCR\alpha\beta^+$ innate-like T cells with high cytotoxic potential in mammary tumors called αβILTCKs[32] (Extended Data Fig. 2e). $CD8\alpha\alpha^+$ T cells mostly differentiate in the thymus in response to strong agonists[32–36] and use either TCRαβ or TCRγδ, but mammary $CD8\alpha\alpha^+$ T cells were mostly $TCR\alpha\beta^+$ (Extended Data Fig. 4a). Flow cytometric validation confirmed that gestating and lactating mammary glands displayed a significant increase in the proportion of $CD8\alpha\alpha^+$ and DN T cells and in cell numbers of $CD4^+$ T_{eff}, $CD8^+$ T_{eff}, $CD8\alpha\alpha^+$ T and DN populations (Fig. 1f,g and gating strategy in Extended Data Fig. 4b).

We investigated other T cell populations and, notably, while T_{reg} cells increased during gestation and involution, their levels dropped significantly during lactation (Extended Data Fig. 4c). Unconventional T cell subsets such as γδ T cells, MR1 + MAIT cells and invariant NK T (iNKT) cells were sparse, and to some extent, decreased upon lactation (Extended Data Fig. 4d,e). Thus, mammary gland remodeling is accompanied by distinct changes in T cell populations, including increased $CD4^+$ T_{eff}, $CD8\alpha\beta^+$ T_{eff} and $CD8\alpha\alpha^+$ T cells in lactation.

Mammary T cell populations are located in the epithelium

The expansion of mammary $CD8\alpha\alpha^+$ T cells, an abundant cell type in the intestine, was intriguing. To compare transcriptional similarities of $CD8\alpha\alpha^+$ T cells across tissues, we multiplexed nulliparous and lactating mammary gland, small and large intestine, and spleen from the same mouse into scRNA-seq experiments (Fig. 2a; 25,096 cells, four mice, two independent experiments). At first glance, T cells from the same tissue clustered together suggesting a distinct transcriptional state that was tissue specific (Fig. 2a). However, signatures of effector $CD4^+$, $CD8\alpha\beta^+$ and $CD8\alpha\alpha^+$ T cells were similar across organs (Fig. 2b). Most $CD8\alpha\alpha^+$ T cell genes, *Tyrobp*, *Fcer1g*, *Itgae* and *Gzmb*, displayed similar expression in mammary gland, small intestine and large intestine but not the spleen (Extended Data Fig. 5a). The expression of killer cell lectin-like receptor (KLR) family genes such as *Klra1*, *Klra7*, *Klrb1a* and *Klrb1c*, were higher in mammary $CD8\alpha\alpha^+$ T cells compared to intestinal tissues (Extended Data Fig. 5a). We validated two classical IEL markers by flow cytometry, Ly49a (*Klra1*), a KLR that binds major histocompatibility complex (MHC) I, and CD103 (*Itgae*), an integrin that mediates tissue retention by binding to e-cadherin on epithelial cells. Lactation led to increased Ly49a expression in mammary $CD103^+CD8\alpha\alpha^+$ T cells, consistent with gene expression data; however, $CD103^+CD8\alpha\alpha^+$ T cell proportions were decreased in the small intestine but not mammary gland (Fig. 2c,d and Extended Data Fig. 5b). We also observed a lactation-mediated increase in the expression of markers associated with intestinal IELs (iIELs), such as CD160, CD38 and 2B4 (CD244)[37–39], on mammary $CD8\alpha\alpha^+$ and $CD8\alpha\beta^+$ T cells (Fig. 2d and Extended Data Fig. 5c). Based on the gene signatures and surface-expression profiles, we hypothesized that $CD8\alpha\alpha^+$ T cells in the mammary gland could be IELs. As the defining characteristic of IELs is their residence in the epithelial layer, we surveyed the physical location of mammary T cells. Indeed, we observed $CD8\alpha\alpha^+$ T cells adjacent to both basal ($Krt14^+$) and luminal ($Krt8^+$) epithelial cells by immunofluorescence (Fig. 2e and Extended Data Fig. 5d). Notably, mammary $CD4^+$ and $CD8\alpha\beta^+$ T cells

https://doi.org/10.1038/s41590-025-02218-3

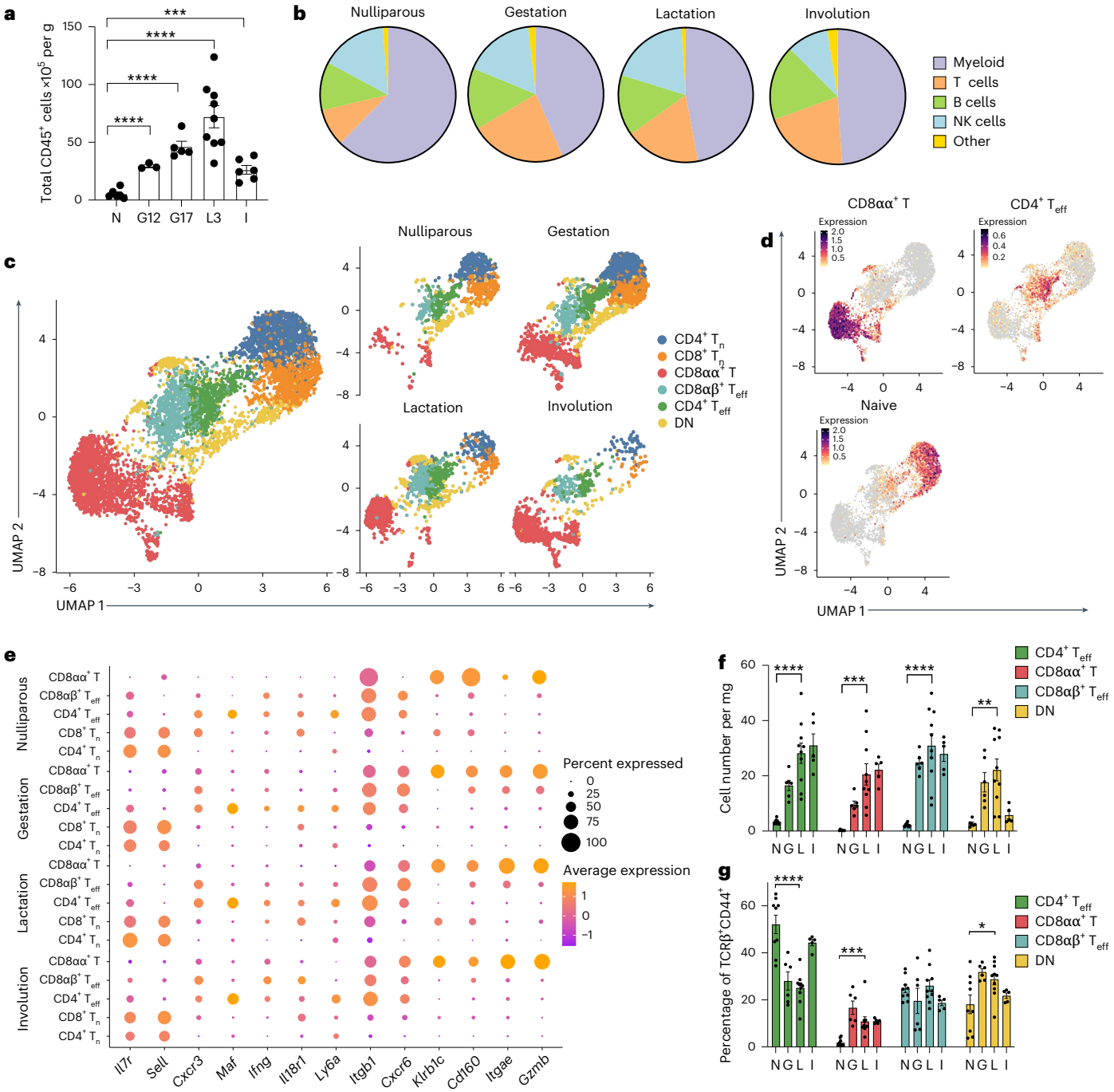

Fig. 1 | Late gestation and lactation lead to increased T cell populations in the mammary gland. a, Quantification of total number of CD45$^+$ cells normalized to mammary gland weight across stages of gestation and lactation by flow cytometry. N, nulliparous ($n = 6$); G12, gestation day 12 ($n = 3$); G17, gestation day 17 ($n = 5$); L3, lactation days 3–5 ($n = 9$); I, involution, 1 day post-weaning ($n = 6$). **b**, Representative proportions of major immune cell types in the mammary gland across stages, N ($n = 5$), G ($n = 3$), L ($n = 5$) and I ($n = 5$) quantified by flow cytometry. **c**, Uniform Manifold Approximation and Projection (UMAP) projection of mammary T cells. Split by stages, N, G17, L3 and I (right). The representative UMAP is from one of three independent experiments, $n = 3$. **d**, Feature plots of CD8αα T, CD4 T_{eff} and T_n cells from **c**. **e**, Dot plot of selected highly expressed genes in T cell clusters across stages identified in **c**. Dot size represents the percentage of cells expressing the selected gene and color indicates expression level. **f**,**g**, Quantification by flow cytometry of cell numbers (**f**) and proportions (**g**) of T cell populations identified in **c** normalized to mammary gland weight. T cell populations were determined as CD4 T_{eff}, CD4$^+$CD44$^+$CD62L$^-$; CD8αα T, CD8α$^+$CD8β$^-$CD44$^+$CD62L$^-$; CD8αβ T_{eff}, CD8α$^+$CD8β$^+$CD44$^+$CD62L$^-$; and DN, TCRβ$^+$CD4$^-$CD8α$^-$. N ($n = 8$, $n = 6$ for DN); G ($n = 6$); L ($n = 10$); and I ($n = 5$). Two-tailed unpaired Student's *t*-tests were performed on the results shown in **a**,**f**,**g**. $^*P < 0.05$, $^{**}P < 0.01$, $^{***}P < 0.001$, $^{****}P < 0.0001$. Data are representative of ≥3 independent experiments. Bars in plots indicate mean ± s.e.m.

were also intraepithelial in location (Fig. 2e and Extended Data Fig. 5d), reminiscent of mucosal epithelium. Overall, our results demonstrate that mammary CD8αα$^+$ T cells have marked phenotypic similarity to intestinal CD8αα$^+$ IELs. The increase in mammary IELs (mIELs) in lactation is indicative of a temporary mucosal state of the reconfigured mammary gland.

https://doi.org/10.1038/s41590-025-02218-3

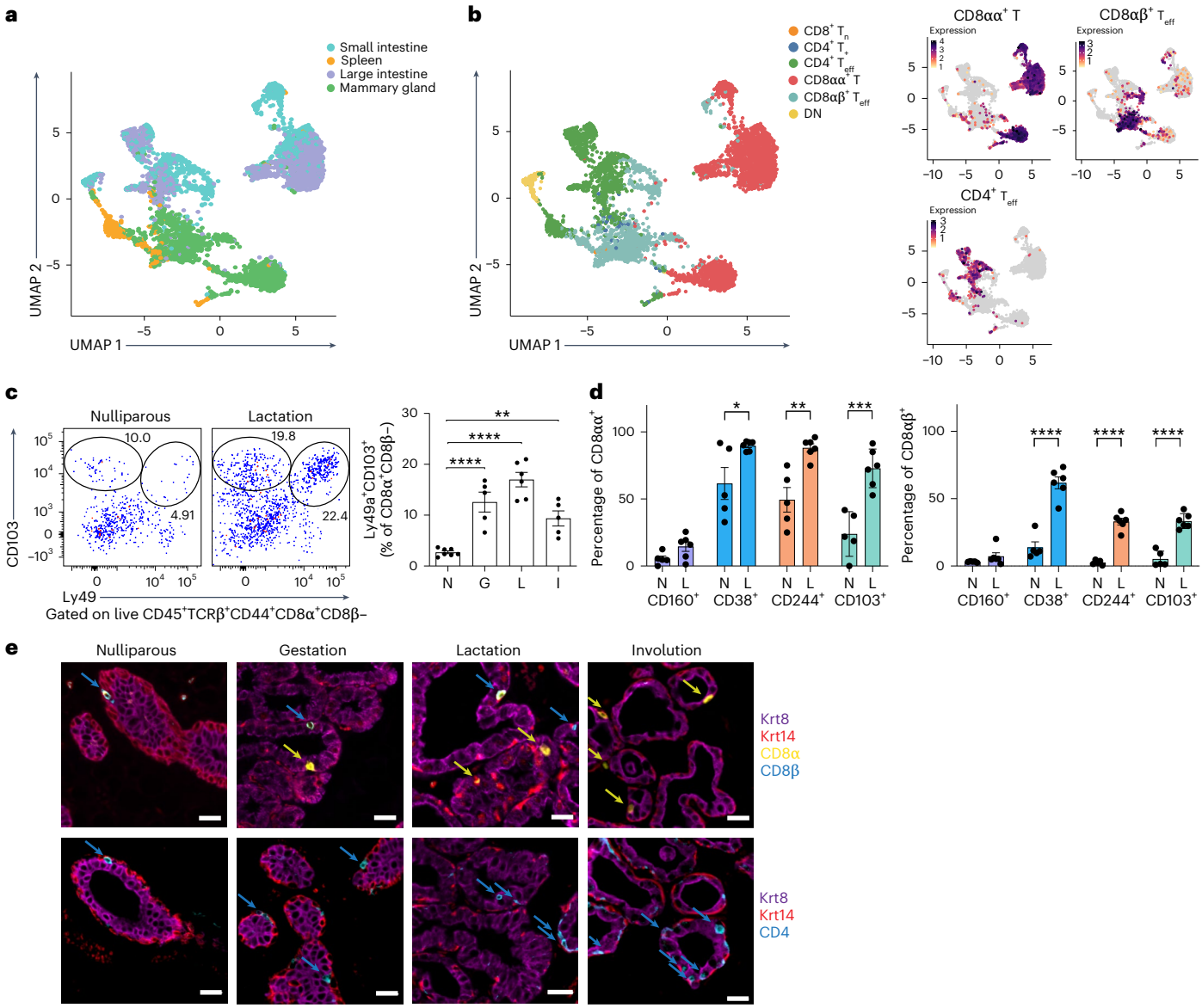

Fig. 2 | Mammary T cells are intraepithelial lymphocytes. a, Summary UMAP projections of T cells from mammary gland, large intestine, spleen and small intestine of lactating mice. **b**, UMAP and feature plots showing the transcriptional localization of featured T cell signatures. **c**, Representative flow cytometry plots and quantification of $CD103^+Ly49^+CD8\alpha\alpha^+$ T cells (gated on live $CD45^+TCR\beta^+CD8\alpha^+CD8\beta^-$) across gestation and lactation stages in the mammary gland. N ($n = 7$), G17 ($n = 5$), L3–5 ($n = 6$) and I, 1 day post-weaning ($n = 5$). **d**, Proportion of $CD8\alpha\alpha^+$ (left) and $CD8\alpha\beta^+$ (right) cells that express CD160, CD38, CD244 and CD103 in N ($n = 5$) and L ($n = 6$) mammary glands. **e**, Representative immunofluorescence images of the mammary gland at N, G17, L3 and I. Epithelial cells ($Krt8^+$ luminal cells in magenta and $Krt14^+$ basal cells in red) and T cells, CD8α in yellow, CD8β in cyan (top) and CD4 in cyan (bottom). Scale bars, 20 µm. Two-tailed unpaired Student's *t*-tests were performed on the results shown in **c**,**d**. $^*P < 0.05$, $^{**}P < 0.01$, $^{***}P < 0.001$, $^{****}P < 0.0001$. Data are representative of ≥3 independent experiments. Bars in plots indicate mean ± s.e.m.

Putative mIEL–epithelial cell interaction networks shift during lactation

Given the intraepithelial location of expanding mammary T cells during lactation, we investigated the potential interaction pathways between mIELs and epithelial cells in nulliparous and lactating mammary glands using CellChat[40] (25,506 cells, four mice per condition). For visualization purposes, we combined ligand–receptor pairs into functionally related signaling pathways (Fig. 3a,b and Extended Data Fig. 6a,c) and plotted communication probabilities between ligand–receptor pairs upregulated (Fig. 3c and Extended Data Fig. 7a) or downregulated (Extended Data Fig. 6b,d) with lactation. Potential interactions that were upregulated with lactation were enriched in pathways related to cell adhesion and migration, including *Pecam1*, selectins (*Sell*), laminins (*Lamb3*) and galectins (*Lgals9*) (Fig. 3a,d). Expression of *Lgals9* and *Lamb3* transcripts was increased in $CD8\alpha\alpha^+$ and $CD8\alpha\beta^+$ IELs, whereas *Pecam1* and *Sell* expression was increased in $CD4^+$ IELs and DN T cells (Fig. 3d). Of note, *Sell* was highly expressed in nulliparous $CD8\alpha\beta^+$ IELs, but its potential interacting partner shifted from *Podxl* in nulliparous mice to *Glycam1* in lactation (Fig. 3c and Extended Data Fig. 6b). *Glycam1* is a mucin-like glycoprotein produced by luminal cells in a prolactin-dependent manner[41] and could potentially facilitate epithelial–IEL interactions during lactogenesis.

Predicted interactions from epithelial cells to mIELs were enriched for immunoregulatory pathways in lactation, including increased expression of MHCs in basal epithelial cells with MHC I signaling to

https://doi.org/10.1038/s41590-025-02218-3

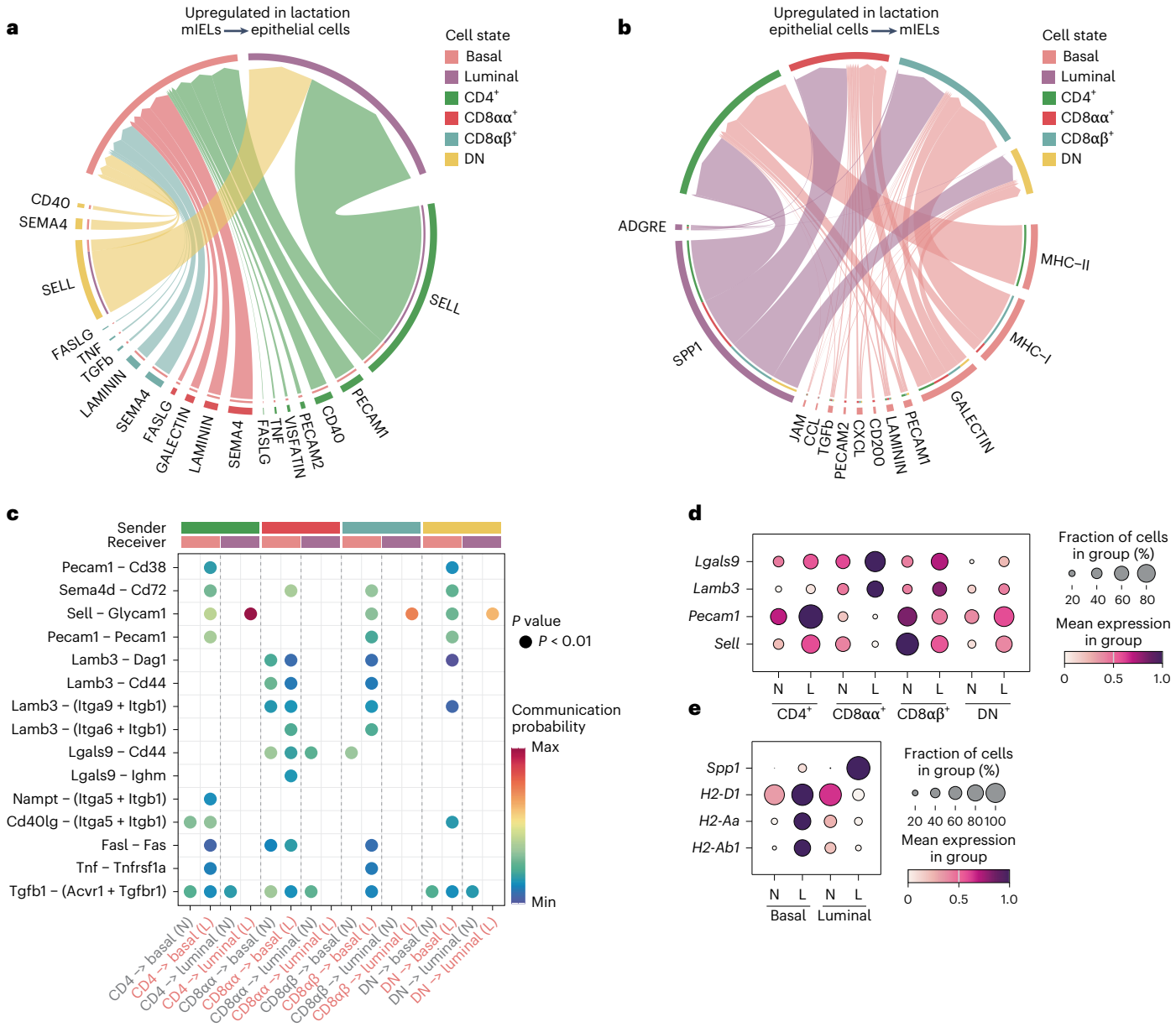

Fig. 3 | Putative interaction networks between mIELs and epithelial cells. **a**,**b**, Chord diagrams showing potential signaling pathways upregulated in lactation from mIEL populations to epithelial cells (**a**) and from epithelial cells to mIEL populations (**b**). Ligand–receptor pairs as summarized into functionally related signaling pathways. Outer thicker bars represent the cell population that is the source or target of the signaling pathway in the chord diagram. The inner thinner bar color is the target of the signal. The thickness of the edge represents the signaling strength (communication probability) as calculated by CellChat. **c**, Dot plot showing the communication probabilities of ligand–receptor pairs upregulated in lactation from mIELs to epithelial cells. Heatmap depicts the communication probability of each ligand pair for each cell pair in N and L3 mammary glands. Sender and receivers are indicated by the color bars on top. *P* values computed by CellChat v.2 from a one-sided permutation test. **d**,**e**, Dot plot of transcript expression levels in mIELs (**d**) and epithelial cells (**e**) in N and L3 mammary glands, depicting the percent of cells expressing and mean expression levels in each cell population. Data are generated using scRNA-seq of epithelial and mIEL populations in N ($n = 2$) and L3 (day 3 postpartum) ($n = 2$) mammary glands.

CD8αα$^+$ and CD8aβ$^+$ mIELs and MHC II signaling to CD4$^+$ mIELs (Fig. 3b,e and Extended Data Fig. 7). In contrast, luminal epithelial cells downregulated MHC complexes during lactation, possibly due to a functional shift toward milk production (Fig. 3e and Extended Data Fig. 6c,d). Another strongly predicted interaction between luminal cells and mIEL populations involves osteopontin (*Spp1*), a glycoprotein associated with epithelial cell proliferation and local immunity during lactation[42] (Fig. 3b,e and Extended Data Fig. 7). Thus, putative interaction analysis suggests multiple signaling pathways between epithelial cells and mIELs, which could regulate immune surveillance and lactogenesis, providing candidates for future functional studies.

T cells migrate from the intestine during gestation

Intestinal TCRαβ$^+$CD8αα$^+$ IELs arise from thymic progenitors acquiring their effector program and expression of gut-homing receptors in the thymus following agonist stimulation by self-antigens[32–36]. To test whether CD8αα$^+$ mIEL increase stemmed directly from the thymus, we thymectomized 4-week-old female mice before pregnancy and assessed CD8αα$^+$ mIELs during lactation. Of note, there were no differences between thymectomized and control mice in numbers of CD8αα$^+$ mIELs or other mIEL subsets in the lactating mammary gland (Fig. 4a) despite the decrease in T cells in mammary gland draining lymph nodes (Extended Data Fig. 8a). While the lack of difference in mIELs could be

https://doi.org/10.1038/s41590-025-02218-3

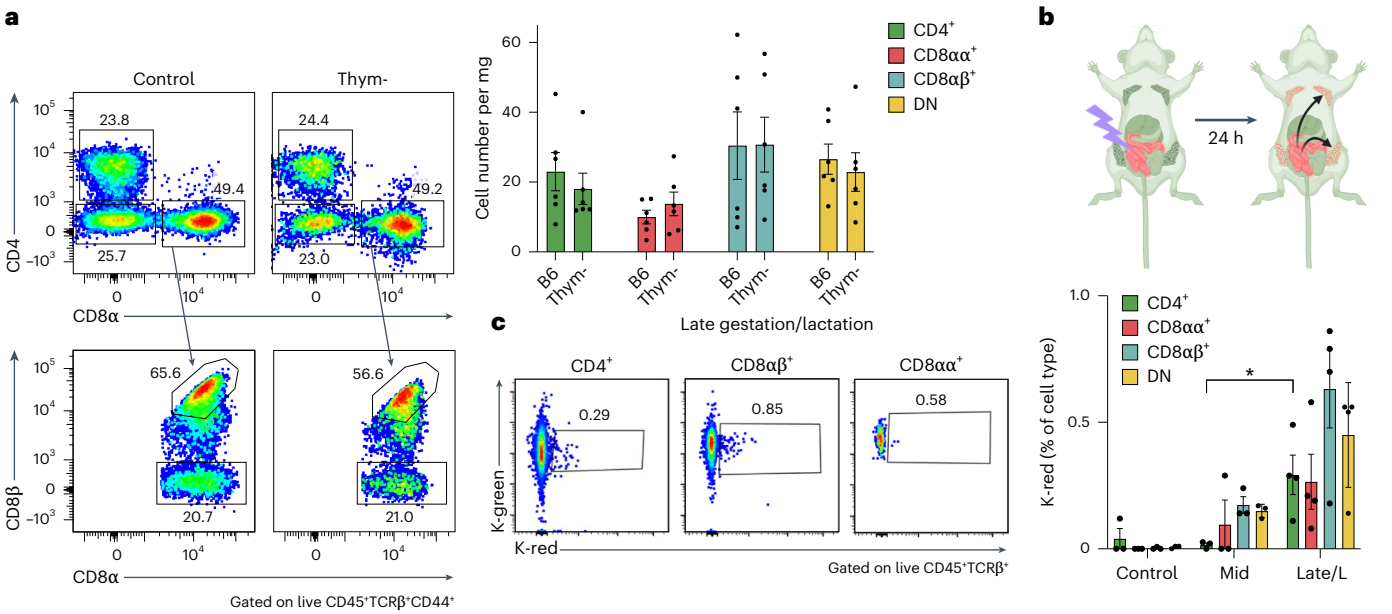

Fig. 4 | Intestinal T cells migrate to the mammary gland during late gestation and lactation. a, Representative flow cytometry plots and quantification of mIEL populations in control B6 ($n = 6$) and thymectomized ($n = 6$) lactating mice. mIEL populations were determined as CD4, $CD4^+CD44^+CD62L^-$; CD8αα, $CD8\alpha^+CD8\beta^-CD44^+CD62L^-$; CD8αβ, $CD8\alpha^+CD8\beta^+CD44^+CD62L^-$; and DN, $TCR\beta^+CD4^-CD8\alpha^-$. **b**, Experimental design for Kaede experiments. Intestines of Kaede-positive mice were photoconverted from green to red by illumination with UV light after laparotomy in mid–late pregnancy and early lactation, and migration of red cells to the mammary gland was examined after 24 h. **c**, Representative flow cytometry plots and quantification of Kaede red cells within T cell populations (gated on $TCR\beta^+$ followed by either $CD4^+$, $CD8\beta^+$, $CD8\alpha^+CD8\beta^-$ or DN) in the mammary gland of mice 24 h post-photoconversion of the intestine. Controls are non-photoconverted mice ($n = 3$), 'mid' are mice photoconverted on gestation day 10 and analyzed on gestation day 11 ($n = 3$) and 'late/L' represents mice both photoconverted on gestation day 16 and analyzed on gestation day 17 and mice photoconverted on lactation day 1 and analyzed on lactation day 2 ($n = 4$). Two-tailed unpaired Student's *t*-tests were performed on the results shown in **a** and **c**. $^*P < 0.05$. Data are representative of ≥3 independent experiments. Bars in plots indicate mean ± s.e.m. Panel **b** created with BioRender.com.

due to compensatory mechanisms in the absence of the thymus, it also raises other possibilities: either thymic progenitors seed the mammary gland before 4 weeks of age and these few T cells expand into $CD8\alpha\alpha^+$ mIELs during pregnancy, or a proportion of $CD8\alpha\alpha^+$ mIELs could be from extrathymic sources, potentially from other mucosal sites, and migrate to the mammary gland during late pregnancy. In the mammary gland, we found a modest increase in $Ki67^+$ T cells during gestation, but not lactation, suggesting that the expansion of mammary T cells could be a combination of proliferating mIELs of thymic origin and extrathymic input (Extended Data Fig. 8b). We previously used Kaede photoconvertible mice to track the migration of immunocytes from the intestines to other body locations[43]. A small population of migratory iIEL-like $TCR\alpha\beta^+CD8\alpha\alpha^+$ cells were found in the spleen[43], which led us to hypothesize that mammary $CD8\alpha\alpha^+$ IELs could be of intestinal origin. To test this hypothesis, intestinal sections (excluding Peyer's patches) of Kaede mice were photoconverted from green to red, at different times of gestation and early lactation, and mammary glands were analyzed 24 h later (Fig. 4b). Notably, due to the challenges associated with performing surgery in pregnant mice, only a portion of the intestine, accessible with minimal disturbance to surrounding tissues, was photoconverted. Kaede red cells of intestinal origin including all three $CD8\alpha\alpha^+$, $CD4^+$ and $CD8\alpha\beta^+$ T cell types had indeed migrated to the mammary gland (Fig. 4c) and spleen as previously reported[43] (Extended Data Fig. 8c). Although these numbers may seem low, they are comparable to the well-established migration of plasma cells from the intestine to the mammary gland, where 1–2% of Kaede red plasma cells migrate over 48 h[18–22]. Thus, expansion of mammary T cells in late pregnancy and lactation is driven by both thymic and intestinal inputs.

T cell clones are shared between iIELs and mIELs

To further establish the relationship between iIELs and mIELs, we analyzed the αβTCR clonotypes expressed by T cells in the small and large intestine, mammary gland and spleen. We used single-cell TCR-seq to compare αβTCR pairs displayed by IELs across tissues between nulliparous and lactating mice (eight mice, 21,750 total cells). Overall, the data showed unremarkable V and J region usage, CDR3 length and N region diversity frequencies. Canonical TRAV11/TRAJ18 TCRs of iNKT cells were relatively abundant among lactating mammary T cells, mostly in $CD4^-CD8^-$ DNs (2.2 and 8.1% of total cells; Extended Data Fig. 9a). Rarefaction analysis revealed a notable degree of clonal amplification across different T cell types from the lactating mammary gland compared to the nulliparous mammary gland, whereas amplification is seen in both the lactating and nulliparous small intestine (Fig. 5a and Extended Data Fig. 9b), but with much mouse-to-mouse variation. We identified 13 TCR clonotypes shared between small intestine and mammary T cells in lactating mice, versus 3 in nulliparous mice (Fig. 5b,c and Supplementary Table 1). These shared clonotypes were defined by full nucleotide sequence identity and were absent across different mice, indicating that they stemmed from the same T cell clones present in both mammary gland and small intestine (and large intestine, for some). Clonotypes shared with the intestines accounted for 4.3% and 0.6% of mIELs in the two lactating mice, certainly an underestimate given incomplete sampling. As indicated in Fig. 5c and Supplementary Table 1, shared clonotypes belonged to several cell types, indicating that the exchange between tissues involves different T lineages. Some clonotypes shared between intestine and mammary gland were also observed in nulliparous females (2.2% and 0.9% of mIELs in the two mice profiled) indicating that T cell exchange between the intestine and mammary gland pre-exists the onset of lactation.

These clonotypic analyses also revealed the sharing of a particular group of cells. For a broader comparison of small intestine cells, we leveraged TCR sequence data of iIELs generated in the ImmGenT program[44], and used the TCRdist3 algorithm[45] to compute a matrix of distances between αβTCR clonotypes. This revealed two prominent

https://doi.org/10.1038/s41590-025-02218-3

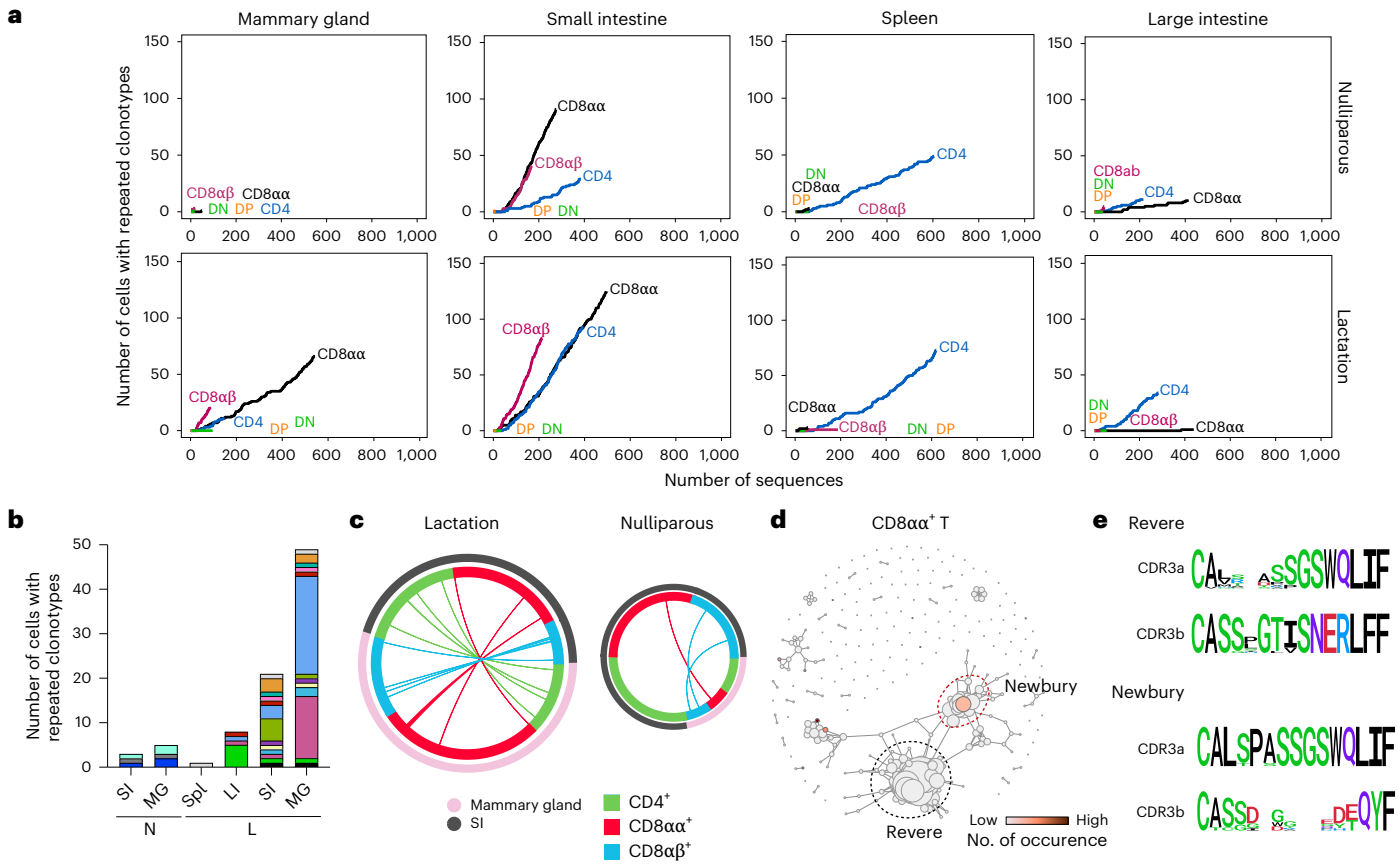

f

	Mouse	Tissue	Cell type	Va	Ja	CDR3α	Vb	Jb	CDR3β
Newbury	m1	SI IEL	CD8αα	TRAV12-2	TRAJ22	CALSASSGSWQLIF	TRBV13-1	TRBJ2-7	CASSDFGGFHEQYF
	m2	SI IEL	CD8αα	TRAV12-3	TRAJ22	CALTPASSGSWQLIF	TRBV13-1	TRBJ2-7	CASSDTGGEYEQYF
	m2	SI IEL	CD8αα	TRAV12-3	TRAJ22	CALSPASSGSWQLIF	TRBV13-1	TRBJ2-5	CASSDADREDTQYF
	m3	Lact MG	CD8αα	TRAV12-3	TRAJ22	CALTPASSGSWQLIF	TRBV3	TRBJ2-4	CASSPTASQNTLYF
	m3	Lact MG	CD8αα	TRAV12-2	TRAJ22	CALSASSGSWQLIF	TRBV13-2	TRBJ2-3	CARTGTEAETLYF
	m3	Lact MG	DN	TRAV12-2	TRAJ22	CALSASSGSWQLIF	TRBV13-1	TRBJ2-7	CASSEGLSSYEQYF
Revere	m2	SI IEL	CD8αα	TRAV6-2	TRAJ22	CVLGASSGSWQLIF	TRBV3	TRBJ1-4	CASSPGTISNERLFF
	m2	SI IEL	CD8αα	TRAV16N	TRAJ22	CAMRASSGSWQLIF	TRBV14	TRBJ1-4	CASSPGTISNERLFF
	m1	SI IEL	CD8αα	TRAV7-6	TRAJ22	CAVASSGSWQLIF	TRBV12-1	TRBJ1-4	CASSSGTISNERLFF
	m4	Lact MG	CD8αα	TRAV6D-5	TRAJ22	CVLSSGSWQLIF	TRBV12-1	TRBJ1-4	CASSPGTISNERLFF
	m3	Lact MG	CD8αα	TRAV6-3	TRAJ22	CAMRALSSGSWQLIF	TRBV13-1	TRBJ1-4	CASSPGTISNERLFF
	m4	Lact MG	DN	TRAV7-2	TRAJ22	CAASISGSWQLIF	TRBV3	TRBJ1-4	CASSSGTISNERLFF

g

Tissue	CD8αα+ counts	Revere + Newbury counts	Percentage
SI	6,577	264	4.01
Peritoneal cavity	28	1	3.57
Colon	2,324	3	0.13
Mammary gland	857	4	0.47
Blood	45	0	0.00
Bone marrow	239	0	0.00
Liver	205	0	0.00
LN	54	0	0.00
Lung	108	0	0.00
Salivary gland	45	0	0.00
Spleen	158	0	0.00
Tumor	80	0	0.00
Uterus	258	0	0.00
All other tissues	3,544	4	0.11

Fig. 5 | mIELs share peculiar TCR repertoires with small intestinal T cells. **a**, Rarefaction analysis from TCR sequencing of T cell types between nulliparous and lactating mice in the mammary gland (MG), small intestine (SI), spleen (Spl) and large intestine (LI). **b**, Quantification of the number of cells with repeated clonotypes between organs in N and L3 mice. Each color represents a unique clonotype. **c**, Chord diagrams of L3 and N stages representing clonotype sharing in different IEL populations (inner ring) between the small intestine and mammary gland (outer ring). Each line represents a TCR clonotype. **d**, Distance matrix between αβTCR clonotypes in iIELs. Red circle denotes 'Newbury TCR' and black circle denotes 'Revere TCR'. **e**, CDR3 sequence of Revere and Newbury TCRs. **f**, Table representing instances of Revere and Newbury TCRs in CD8αα$^+$ T cells in mammary gland and small intestine across different mice. **g**, Counts of Revere and Newbury TCRs in CD8αα$^+$ T cells across multiple tissues. Data are representative of ≥3 independent experiments.

TCR families within iIELs (Fig. 5d), whose over-representation was noteworthy because of the recruitment of highly related TCRs with little clonal amplification, as denoted by subtly different nucleotide sequences. These TCR families were found across independent samples, and one corresponded to the previously reported 'Revere' family[46] (we hereafter, name the second family 'Newbury'). Revere TCRs are mostly conserved in the CDR3b region, with exclusive usage of TRAJ22 and TRBJ1-4 (Fig. 5e and Extended Data Fig. 9c), whereas the Newbury family is mostly conserved in the CDR3a region. Notably, these two families are almost exclusively represented in CD8αα$^+$ iIELs, amounting to a few percent of T cells (Extended Data Fig. 9d,e), and these highly identical TCRs of CD8αα$^+$ iIELs are likely selected repeatedly by self-reactivity, in line with selection of CD8αα differentiation by self-reactive transgenic TCRs[34–36]. Of note, Revere and Newbury TCRs were also observed in CD8αα$^+$ IELs of the mammary gland (three of each), with all the key sequence characteristics (Fig. 5f and Extended Data Fig. 9f). Thus, peculiar TCR families of CD8αα$^+$ iIELs are found in mIELs during lactation. Notably, outside of the intestine and mammary gland, CD8αα$^+$ IELs did not display Revere or Newbury family TCRs, as analyzed by the ImmGenT program (Fig. 5g; $P = 6 \times 10^{-4}$,

https://doi.org/10.1038/s41590-025-02218-3

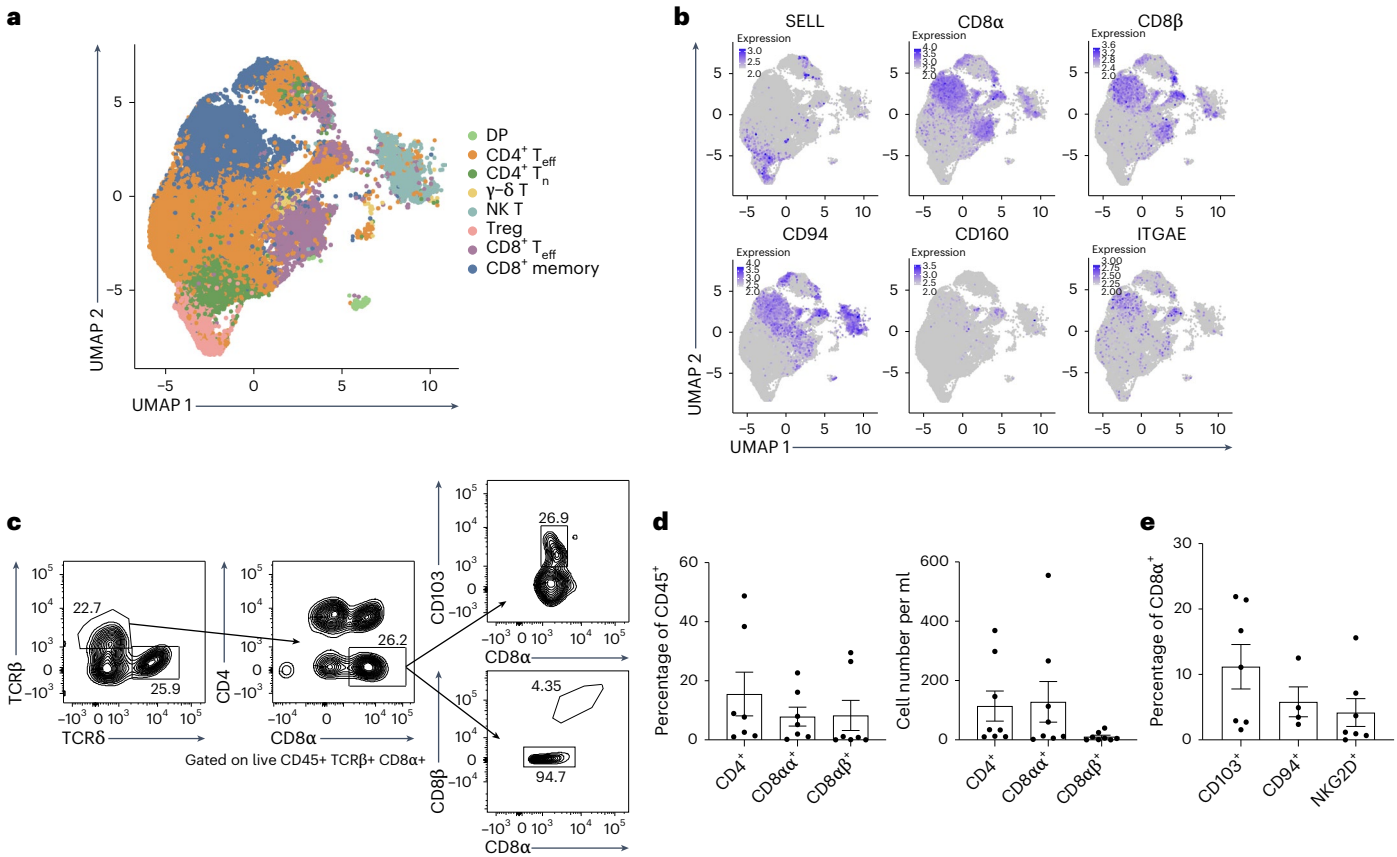

Fig. 6 | mIEL-like cells are found in human breast and milk. a, UMAP projection of mammary immunocytes from human breast tissue (sourced from Kumar et al.[47]). **b**, Feature plots of selected genes projected on UMAP from **a**. **c**, Representative flow cytometry gating of CD8α$^+$CD103$^+$ T cells and CD8αα$^+$ IEL-like cells in human milk samples. **d**, Quantification of CD4$^+$, CD8αα$^+$ and CD8αβ$^+$ cells as percent of CD45$^+$ cells (left) ($n = 7$) and cell number normalized to volume (right) ($n = 8$) in human milk samples. **e**, Proportion of human CD8αα IEL-like cells that express markers CD103 ($n = 7$), CD94 ($n = 4$) and NKG2D ($n = 7$) in human milk samples. Two-tailed unpaired Student's *t*-tests were performed on the results shown in **d** and **e**; no significance was observed. Data represent ≥7 independent milk samples/experiments. Bars in plots indicate mean ± s.e.m. scRNA-seq data were from Kumar et al.[47].

chi-squared test). Together, during lactation, CD8αα$^+$ mIELs displayed TCRs otherwise exclusive to iIELs, as part of a broader exchange of T cell clones between the small intestine and mammary gland.

IEL-like cells are present in human mammary gland and milk

We assessed whether mIELs were conserved across species by profiling T cells in human breast tissue and human milk. We used previously published scRNA-seq datasets[47] and found that human breast tissue from nonlactating women contains naive (*SELL*) T cells as well as CD4$^+$ and CD8αβ$^+$ T cells that express tissue-resident and cytotoxic markers expressed by mouse mIELs, including *ITGAE*, *CD94*, *CD160*, *NKG2D* and *GZMB* (Fig. 6a,b and Extended Data Fig. 10a). We also observed a small population of cells that expressed genes associated with CD8αα$^+$ IELs, including *FCER1G* and *TYROBP*. The presence of CD4$^+$ and CD8$^+$ T cells in milk has been reported before[25], but with no further characterization. To ask whether human milk contains mIEL-like cells, we analyzed fresh milk samples from lactating women. Flow cytometry revealed both CD4$^+$ and CD8$^+$ T cells in all samples. In addition, CD8αα$^+$ mIEL-like cells were present in human milk, including cells that expressed CD103, CD94 and NKG2D (Fig. 6c–e). Overall, we identified human counterparts of mouse mIELs in human breast and milk.

Microbiota influence numbers of mIELs

The classical function of IELs is to maintain barrier immunity, which raised the question of microbe-dependence of IELs in the lactating mammary gland. Lactating mammary glands in microbe-deficient germ-free (GF) mice had morphologically different ducts compared to microbe-sufficient (specific pathogen free; SPF) control mice (Fig. 7a). Although the number of mammary alveoli in SPF and GF mice were comparable, the average area (μm^2) of GF alveoli was larger, indicating that microbes may affect the developmental progression of the mammary gland during lactation (Fig. 7b,c). Mammary immunocyte numbers were influenced by microbes, as indicated by reduced total CD45$^+$ cells in lactating GF mice, which was comparable to nulliparous SPF mice (Fig. 7d and Extended Data Fig. 10b). There were no differences in proportions of basal and luminal epithelial cells (Extended Data Fig. 10c) or pup weights normalized to litter size in GF versus SPF conditions (Extended Data Fig. 10d), but whether microbes influence milk composition or production needs to be further investigated.

GF mice showed decreased numbers of CD4$^+$, CD8αα$^+$ and CD8αβ$^+$ mIELs compared to SPF mice (Fig. 7e). The decrease in mIEL numbers was due to the total drop in CD45$^+$ cells as proportions of mIEL types were not different between groups (Extended Data Fig. 10e), indicating the involvement of other factors in mammary mIEL recruitment. The decrease in mIELs could stem from decreased iIELs, as GF mice display a substantial decrease in CD4$^+$ iIELs and CD8αβ$^+$ iIELs and a modest decrease in CD8αα$^+$ iIELs[48]. The defect in mIELs may also arise from migrating iIELs that lack the same functionality or an indirect effect of microbes on factors that promote iIEL differentiation and proliferation. To test the role of intestinal microbes, we conventionalized GF mice by transferring fecal microbes from control SPF mice into GF mice at 6 weeks of age. Conventionalized GF mice displayed

https://doi.org/10.1038/s41590-025-02218-3

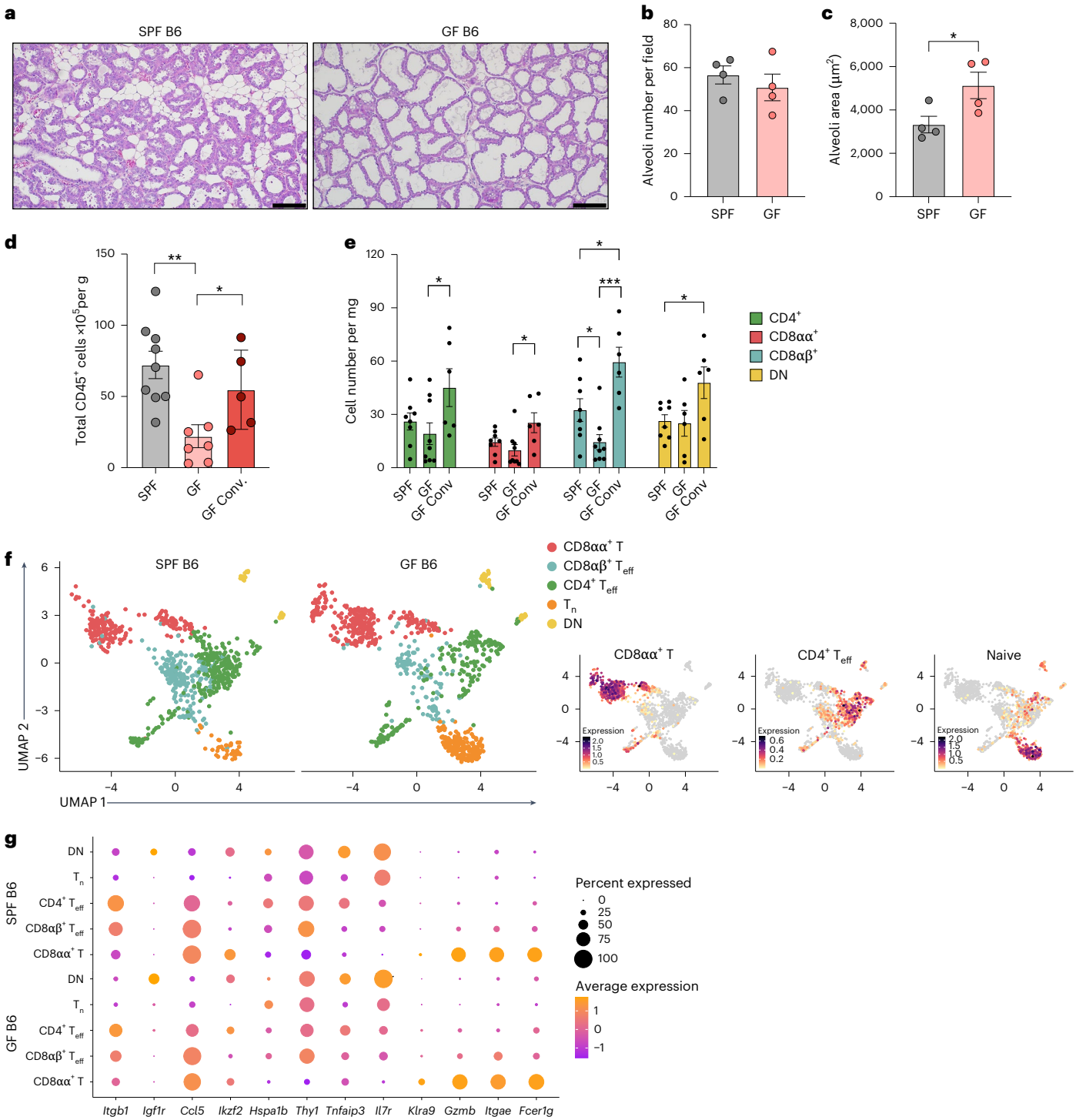

Fig. 7 | mIEL expansion in the lactating mammary gland is partially dependent on microbes. a, Representative hematoxylin and eosin (H&E) staining of lactating mammary glands from SPF and GF mice. Scale bars, 100 µm. **b**,**c**, Quantification of the average number (**b**) and average area (µm²) (**c**) of alveoli per ×20 image fields (five images per mouse of size 900 × 500 µm) of SPF and GF mammary glands ($n = 4$). **d**, Quantification of the total number of CD45⁺ cells normalized to mammary gland weight in SPF ($n = 9$), GF ($n = 7$) and GF conventionalized mice ($n = 5$). **e**, Quantification of total cell numbers normalized to mammary gland weight, of specified mIEL populations in SPF ($n = 8$), GF ($n = 9$, $n = 6$ for DN) and GF conventionalized ($n = 6$) mice by flow cytometry. mIEL populations were determined as CD4, CD4⁺CD44⁺CD62L⁻; CD8αα, CD8α⁺CD8β⁻CD44⁺CD62L⁻; CD8αβ, CD8α⁺CD8β⁺CD44⁺CD62L⁻; and DN, TCRβ⁺CD4⁻CD8α⁻. **f**, UMAP projection of mIELs from lactating SPF and GF mice with feature plots of naive, CD4 effector and CD8αα T cell gene signatures. **g**, Dot plot of differentially expressed genes in mIEL populations between lactating SPF and GF mice from **f**. Two-tailed unpaired Student's *t*-tests were performed on the results shown in **b**–**e**. $^{*}P < 0.05$, $^{**}P < 0.01$ $^{***}P < 0.001$. Data are representative of ≥3 independent experiments. Bars in plots indicate mean ± s.e.m.

increased CD45⁺ cells during lactation, including restoration of the mIEL populations (Fig. 7d,e). To further analyze microbe-dependent phenotypic changes, we performed multiplexed scRNA-seq on T cells from lactating mammary glands from GF or SPF mice (Fig. 7f; 13,021 cells, eight mice and two independent runs). All mIEL populations were equally represented in the two groups consistent with quantitation

by flow cytometry (Fig. 7f). Differential gene expression between SPF and GF IELs showed few transcriptional differences; however, there were some notable changes in *Itgb1*, *Igf1r*, *Ikzf2*, *Tnfaip3*, *Thy1* and *Klra9* (Fig. 7g). While several of these genes are immunomodulatory, whether these changes affect the function of mIELs in GF mice needs to be examined. Thus, our data points to the role of commensal microbes in modulating numbers of total CD45$^+$ cells, including mIELs during lactation.

Discussion

We report a dynamic atlas of mammary T cells whose changes accompany the adaptation of the mammary gland to a mucosal state in lactation, marked by an increase in activated intraepithelial CD4$^+$, CD8αβ$^+$ and CD8αα$^+$ T cells. mIELs shared TCR clonotypes with iIELs, suggesting T cell migration between the intestine and the mammary gland. T cells with a similar mIEL signature were present in human breast tissue and milk indicating conservation across species. Finally, we found that mIEL numbers in lactation were partly influenced by the presence of microbes, suggesting that the observed mIEL changes could play a role in promoting barrier immunity.

Given the barrier-protective functions of iIELs[31], mIELs may serve a similar role to support the mucosal state in the mammary gland during lactogenesis. The TCR specificity of CD8αα$^+$ IELs is directed toward self-antigens[34–36], and we found two families of TCRs that are repeatedly generated and selected across mice in the small intestine and lactating mammary gland. CD8αα homodimers have been shown to function as TCR corepressors by binding to the thymus leukemia antigen on epithelial cells to negatively regulate T cell activation by decreasing antigen sensitivity, in contrast with CD8αβ heterodimers that enhance TCR function[49]. Our results suggest that CD8αα$^+$ mIELs are poised to respond to the rapid epithelial cell proliferation, or to the plethora of self-antigens that are present in the lactating mammary gland, but whether their function is tolerogenic or cytotoxic needs to be determined. A recent study reported that thymic IEL precursors are redirected from the intestine to the mammary gland during pregnancy, where they differentiate into mIELs and promote lactogenesis by regulating mammary epithelial cells and milk production[50]. The redirection of thymic precursors is intriguing and could complement our observations, where the factors that aid the re-routing of IEL precursors from thymus to mammary gland might also drive the gut–mammary migration of IELs. During pregnancy, the expression of gut-homing markers Ccl25, Ccl28 and MAdCAM1 increase in the mammary tissue, which could recruit T cells to the mammary gland[22,51,52]; however, whether the expression of these homing markers change in the intestine during pregnancy to mediate T cell egress and whether hormones influence mammary-homing markers need to be further explored.

Apart from their physiological role in lactogenesis, CD8αα$^+$ IELs may influence post-lactation oncogenesis. Similar populations of NK-like unconventional T cells such as αβILTCKs and NK-like γδ T cells have been shown to be important in suppressing mammary oncogenesis[26,32]. Mammary T cells are present in human milk where their function, if any, is unclear. One possibility is that their presence is passive and linked to epithelial cell sloughing in lactogenesis, increasing epithelium-associated T cells in milk. Maternal T cells have previously been suggested to colonize neonatal intestines[53], raising another possibility that mIELs in milk could migrate into and colonize the neonatal intestine to promote barrier protection; however, this requires further investigation.

While pregnancy induces an immunosuppressive state to maintain maternal–fetal tolerance[54], we observed increased mammary effector T cells in late pregnancy and lactation, likely preparing for epithelial expansion and microbial exposure. Consistent with the idea of increased microbial exposure, the drop in mammary T_{reg} cells in lactating SPF mice is not observed in GF mice (Extended Data Fig. 10f). Notably, liMacs were reduced in lactating GF mammary glands[17], suggesting that microbes or microbe-derived signals can influence multiple immunocyte types involved in mammary remodeling. Additionally, liMacs protect against infections such as mastitis[17], but whether mIELs influence mastitis susceptibility needs to be further investigated.

In summary, we have characterized T cell changes during lactogenesis and provide evidence for T cell migration potentially along the gut–mammary axis. Our results set the stage for deepening our understanding of T cell function in lactogenesis, which could provide new strategies to improve maternal defense and tolerance during and after lactation.

Online content

Any methods, additional references, Nature Portfolio reporting summaries, source data, extended data, supplementary information, acknowledgements, peer review information; details of author contributions and competing interests; and statements of data and code availability are available at https://doi.org/10.1038/s41590-025-02218-3.

References

1. Joshi, P. A. et al. Progesterone induces adult mammary stem cell expansion. *Nature* **465**, 803–807 (2010).
2. Asselin-Labat, M. L. et al. Control of mammary stem cell function by steroid hormone signalling. *Nature* **465**, 798–802 (2010).
3. Dulbecco, R., Henahan, M. & Armstrong, B. Cell types and morphogenesis in the mammary gland. *Proc. Natl Acad. Sci. USA* **79**, 7346–7350 (1982).
4. Hassiotou, F. & Geddes, D. Anatomy of the human mammary gland: current status of knowledge. *Clin. Anat.* **26**, 29–48 (2013).
5. Watson, C. J. & Khaled, W. T. Mammary development in the embryo and adult: a journey of morphogenesis and commitment. *Development* **135**, 995–1003 (2008).
6. Bach, K. et al. Differentiation dynamics of mammary epithelial cells revealed by single-cell RNA sequencing. *Nat. Commun.* **8**, 2128 (2017).
7. Nyquist, S. K. et al. Cellular and transcriptional diversity over the course of human lactation. *Proc. Natl Acad. Sci. USA* **119**, e2121720119 (2022).
8. Li, M. et al. Mammary-derived signals activate programmed cell death during the first stage of mammary gland involution. *Proc. Natl Acad. Sci. USA* **94**, 3425–3430 (1997).
9. Watson, C. J. Involution: apoptosis and tissue remodelling that convert the mammary gland from milk factory to a quiescent organ. *Breast Cancer Res.* **8**, 203 (2006).
10. Lilla, J. N. & Werb, Z. Mast cells contribute to the stromal microenvironment in mammary gland branching morphogenesis. *Dev. Biol.* **337**, 124–133 (2010).
11. Gouon-Evans, V., Rothenberg, M. E. & Pollard, J. W. Postnatal mammary gland development requires macrophages and eosinophils. *Development* **127**, 2269–2282 (2000).
12. Dawson, C. A. et al. Tissue-resident ductal macrophages survey the mammary epithelium and facilitate tissue remodelling. *Nat. Cell Biol.* **22**, 546–558 (2020).
13. O'Brien, J., Martinson, H., Durand-Rougely, C. & Schedin, P. Macrophages are crucial for epithelial cell death and adipocyte repopulation during mammary gland involution. *Development* **139**, 269–275 (2012).
14. Pollard, J. W. & Hennighausen, L. Colony stimulating factor 1 is required for mammary gland development during pregnancy. *Proc. Natl Acad. Sci. USA* **91**, 9312–9316 (1994).
15. Ingman, W. V., Wyckoff, J., Gouon-Evans, V., Condeelis, J. & Pollard, J. W. Macrophages promote collagen fibrillogenesis around terminal end buds of the developing mammary gland. *Dev. Dyn.* **235**, 3222–3229 (2006).

16. Reed, J. R. & Schwertfeger, K. L. Immune cell location and function during post-natal mammary gland development. *J. Mammary Gland Biol. Neoplasia* **15**, 329–339 (2010).
17. Cansever, D. et al. Lactation-associated macrophages exist in murine mammary tissue and human milk. *Nat. Immunol.* **24**, 1098–1109 (2023).
18. Ramanan, D. et al. An immunologic mode of multigenerational transmission governs a gut Treg setpoint. *Cell* **181**, 1276–1290 e1213 (2020).
19. Roux, M. E., McWilliams, M., Phillips-Quagliata, J. M., Weisz-Carrington, P. & Lamm, M. E. Origin of IgA-secreting plasma cells in the mammary gland. *J. Exp. Med.* **146**, 1311–1322 (1977).
20. Roux, M. E., McWilliams, M., Phillips-Quagliata, J. M. & Lamm, M. E. Differentiation pathway of Peyer's patch precursors of IgA plasma cells in the secretory immune system. *Cell Immunol.* **61**, 141–153 (1981).
21. Lazarus, N. H. et al. A common mucosal chemokine (mucosae-associated epithelial chemokine/CCL28) selectively attracts IgA plasmablasts. *J. Immunol.* **170**, 3799–3805 (2003).
22. Wilson, E. & Butcher, E. C. CCL28 controls immunoglobulin (Ig)A plasma cell accumulation in the lactating mammary gland and IgA antibody transfer to the neonate. *J. Exp. Med.* **200**, 805–809 (2004).
23. Plaks, V. et al. Adaptive immune regulation of mammary postnatal organogenesis. *Dev. Cell* **34**, 493–504 (2015).
24. Betts, C. B. et al. Mucosal immunity in the female murine mammary gland. *J. Immunol.* **201**, 734–746 (2018).
25. Wirt, D. P., Adkins, L. T., Palkowetz, K. H., Schmalstieg, F. C. & Goldman, A. S. Activated and memory T lymphocytes in human milk. *Cytometry* **13**, 282–290 (1992).
26. Hanasoge Somasundara, A. V. et al. Parity-induced changes to mammary epithelial cells control NKT cell expansion and mammary oncogenesis. *Cell Rep.* **37**, 110099 (2021).
27. Butler, A., Hoffman, P., Smibert, P., Papalexi, E. & Satija, R. Integrating single-cell transcriptomic data across different conditions, technologies, and species. *Nat. Biotechnol.* **36**, 411–420 (2018).
28. Crowl, J. T. et al. Tissue-resident memory $CD8^+$ T cells possess unique transcriptional, epigenetic and functional adaptations to different tissue environments. *Nat. Immunol.* **23**, 1121–1131 (2022).
29. Kiner, E. et al. Gut $CD4^+$ T cell phenotypes are a continuum molded by microbes, not by T_H archetypes. *Nat. Immunol.* **22**, 216–228 (2021).
30. Denning, T. L. et al. Mouse TCRαβ+CD8αα intraepithelial lymphocytes express genes that down-regulate their antigen reactivity and suppress immune responses. *J. Immunol.* **178**, 4230–4239 (2007).
31. Cheroutre, H., Lambolez, F. & Mucida, D. The light and dark sides of intestinal intraepithelial lymphocytes. *Nat. Rev. Immunol.* **11**, 445–456 (2011).
32. Chou, C. et al. Programme of self-reactive innate-like T cell-mediated cancer immunity. *Nature* **605**, 139–145 (2022).
33. Ruscher, R. & Hogquist, K. A. Development, ontogeny, and maintenance of $TCR\alpha\beta^+$ CD8αα IEL. *Curr. Opin. Immunol.* **58**, 83–88 (2019).
34. Leishman, A. J. et al. Precursors of functional MHC class I- or class II-restricted $CD8\alpha\alpha^+$ T cells are positively selected in the thymus by agonist self-peptides. *Immunity* **16**, 355–364 (2002).
35. Gangadharan, D. et al. Identification of pre- and postselection TCRαβ+ intraepithelial lymphocyte precursors in the thymus. *Immunity* **25**, 631–641 (2006).
36. Hogquist, K. A., Baldwin, T. A. & Jameson, S. C. Central tolerance: learning self-control in the thymus. *Nat. Rev. Immunol.* **5**, 772–782 (2005).
37. Brenes, A. J. et al. Tissue environment, not ontogeny, defines murine intestinal intraepithelial T lymphocytes. *eLife* **10**, e70055 (2021).
38. Kornberg, A. et al. Gluten induces rapid reprogramming of natural memory αβ and γδ intraepithelial T cells to induce cytotoxicity in celiac disease. *Sci. Immunol.* **8**, eadf4312 (2023).
39. Jaeger, N. et al. Single-cell analyses of Crohn's disease tissues reveal intestinal intraepithelial T cells heterogeneity and altered subset distributions. *Nat. Commun.* **12**, 1921 (2021).
40. Jin, S. et al. Inference and analysis of cell–cell communication using CellChat. *Nat. Commun.* **12**, 1088 (2021).
41. Hou, Z. et al. Glycosylation-dependent cell adhesion molecule 1 (GlyCAM 1) is induced by prolactin and suppressed by progesterone in mammary epithelium. *Endocrinology* **141**, 4278–4283 (2000).
42. Alain, K. et al. Osteopontin: an early innate immune marker of *Escherichia coli* mastitis harbors genetic polymorphisms with possible links with resistance to mastitis. *BMC Genomics* **10**, 444 (2009).
43. Galvan-Pena, S., Zhu, Y., Hanna, B. S., Mathis, D. & Benoist, C. A dynamic atlas of immunocyte migration from the gut. *Sci. Immunol.* **9**, eadi0672 (2024).
44. Zemmour, D., Goldrath, A., Kronenberg, M., Kang, J. & Benoist, C. The ImmGen consortium OpenSource T cell project. *Nat. Immunol.* **23**, 643–644 (2022).
45. Mayer-Blackwell, K. et al. TCR meta-clonotypes for biomarker discovery with tcrdist3 enabled identification of public, HLA-restricted clusters of SARS-CoV-2 TCRs. *eLife* **10**, e68605 (2021).
46. Schattgen, S. A. et al. Intestinal intraepithelial lymphocyte repertoires are imprinted clonal structures selected for MHC reactivity. *Cell Press Sneak Peek* https://doi.org/10.2139/ssrn.3467160 (2019).
47. Kumar, T. et al. A spatially resolved single-cell genomic atlas of the adult human breast. *Nature* **620**, 181–191 (2023).
48. Sujino, T. et al. Tissue adaptation of regulatory and intraepithelial $CD4^+$ T cells controls gut inflammation. *Science* **352**, 1581–1586 (2016).
49. Cheroutre, H. & Lambolez, F. Doubting the TCR coreceptor function of CD8αα. *Immunity* **28**, 149–159 (2008).
50. Corral, D. et al. Mammary intraepithelial lymphocytes promote lactogenesis and offspring fitness. *Cell* **188**, 1662–1680 e1624 (2025).
51. Brandtzaeg, P. The mucosal immune system and its integration with the mammary glands. *J. Pediatr.* **156**, S8–S15 (2010).
52. Low, E. N., Zagieboylo, L., Martino, B. & Wilson, E. IgA ASC accumulation to the lactating mammary gland is dependent on VCAM-1 and α4 integrins. *Mol. Immunol.* **47**, 1608–1612 (2010).
53. Cabinian, A. et al. Transfer of maternal immune cells by breastfeeding: maternal cytotoxic T lymphocytes present in breast milk localize in the Peyer's patches of the nursed infant. *PLoS ONE* **11**, e0156762 (2016).
54. Erlebacher, A. Immunology of the maternal-fetal interface. *Annu. Rev. Immunol.* **31**, 387–411 (2013).

ImmgenT consortium

Aaron Liu[1], Alexander Chervonsky[9], Alexandra Cassano[9], Alia Welsh[10], Ananda Goldrath[11], Andrea Lebron-Figueroa[3], Ankit Malik[9], Anna-Maria Globig[1], Antoine Freuchet[9], Bana Jabri[9], Charlotte Imianowski[12], Claire Thefane[13], Dan Kaplan[12], Dania Mallah[3], Dario Vignali[12], David Sinclair[3], David Zemmour[9], Derek Bangs[14], Domenic Abbondanza[9], Enxhi Ferraj[15], Eric Weiss[12], Erin Lucas[13], Evelyn Chang[15], Gavyn Bee[16], Giovanni Galleti[2], Iliyan Iliev[17], Jinseok Park[3], Joonsoo Kang[15], Jordan Voisine[9], Josh Choi[3], Julia Merkenschlager[18], Jun Huh[3], Katharine Block[13], Ken Cadwell[16], Kevin Osum[13], Laurent Brossay[19], Laurent Gapin[20], Liang Yang[3], Lizzie Garcia-Rivera[1], Marc Jenkins[13], Maria Brbic[21], Marion Pepper[14], Marisa Alegre[9], Mariya London[22], Matthew Stephens[9], Maurizio Fiusco[21], Melanie Vacchio[10], Michael Starnbach[3], Michel Nussenzweig[18], Mitchell Kronenberg[23], Myriam Croze[24], Nalat Siwapornchai[3], Nathan Morris[17], Nika Abdollahi[24], Niket Patel[3], Odhran Casey[3], Olga Barreiro[3], Paul Thomas[25], Peter Carbonetto[9], Remy Bosselut[10], Rocky Lai[15], Sam Behar[15], Sam Borys[19], Sara Quon[2], Serge Candéias[26], Shanelle Reilly[19], Shanshan Zhang[3], Siba Smarak Panigrahi[21], Sofia Kossida[24], Stefan Muljo[10], Stefan Schattgen[25], Stefani Spranger[27], Steve Jameson[13], Susan Kaech[1], Takato Kusakabe[17], Taylor Heim[27], Tianze Wang[14], Tomoyo Shinkawa[15], Ulrich von Andrian[3], Val Piekarsa[3], Véronique Giuducelli[24], Vijay Kuchroo[3] & Woan-Yu Lin[17]

[9]The University of Chicago, Chicago, IL, USA. [10]National Institutes of Health, Bethesda, MD, USA. [11]Allen Institute for Immunology, Seattle, WA, USA. [12]University of Pittsburgh, Pittsburgh, PA, USA. [13]University of Minnesota, Minnesota, MN, USA. [14]University of Washington, Seattle, WA, USA. [15]University of Massachusetts Chan Medical School, Worcester, MA, USA. [16]University of Pennsylvania, Philadelphia, PA, USA. [17]Weill Cornell Medical School, New York, NY, USA. [18]The Rockefeller University, New York, NY, USA. [19]Brown University, Providence, RI, USA. [20]University of Colorado, Boulder, CO, USA. [21]Swiss Federal Institute of Technology, Lausanne, Switzerland. [22]New York University, New York, NY, USA. [23]La Jolla Institute for Immunology, La Jolla, CA, USA. [24]University of Montpellier, Montpellier, France. [25]St. Jude Children's Research Hospital, Memphis, TN, USA. [26]French Alternative Energies and Atomic Energy Commission, Paris-Saclay, France. [27]Massachusetts Institute of Technology, Cambridge, MA, USA.

https://doi.org/10.1038/s41590-025-02218-3

Methods

Mice

C57BL/6 (B6) mice were purchased from The Jackson Laboratory and maintained in SPF conditions at Harvard Medical School and Salk Institute for Biological Sciences. Nulliparous mice were littermate controls of mice profiled at pregnancy, lactation or involution. For timed pregnancies, female B6 mice were set up at 6–8 weeks of age with male B6 mice, female mice with plugs were separated and housed individually for the duration of pregnancy and mammary glands were profiled at day 12 (G12), day 17 (G17) of pregnancy, lactation day 3–5 (L3) and involution day 1 (I), 1 day post-weaning of pups at day 21.

GF B6 mice were purchased at the time points listed above from the University of California San Diego (UCSD). GF mice were conventionalized by oral gavage of fecal microbiota from SPF B6 mice, 1 week before mating and maintained in SPF conditions.

Kaede reporter mice were obtained from O. Kanagawa (RIKEN) and maintained on a B6 background[55,56].

All experiments were performed following the guidelines listed in animal protocols (IS00001257, Harvard Medical School) and (23-00007, Salk Institute for Biological Studies) approved by the Institutional Animal Care and Use Committee. Mice were bred and housed on a 12-h light–dark cycle, maintained at a temperature of 22–24 °C and relative humidity of 45–65%.

Preparation of lymphocytes and flow cytometry

Mammary gland. Inguinal lymph nodes were removed and mammary glands 3, 4 and 5 were collected, minced and dissociated in collagenase solution (3 mg ml^{-1} collagenase type II (Sigma C6885) and 2% FBS in Dulbecco's modified Eagle's medium; DMEM) in a 37 °C shaking water bath for 20 min with manual shaking every 5 min, followed by red blood cell lysis. Single-cell suspensions were filtered and washed with 2% DMEM solution.

Thymus and LN. Lymphocytes from thymus and inguinal lymph nodes were obtained by mechanical disruption, filtered and washed with 10% RPMI solution.

Intestines. Small and large intestinal tissues were measured, cleaned and treated with RPMI containing 1 mM dithiothreitol (DTT), 20 mM EDTA and 2% FBS at 37 °C for 15 min to isolate the epithelial and IEL fractions. For the lamina propria (LP) fraction, the remaining tissue was dissociated in collagenase solution (1 mg ml^{-1} collagenase VIII (Sigma C2139), 50 µg ml^{-1} DNase (Sigma C6885) in 1% FBS in RPMI) with constant stirring at 37 °C for 30 min. Single-cell suspensions for the IEL and LP fractions were filtered and washed with 10% RPMI solution.

Spleen. Tissue was mechanically disrupted, followed by red blood cell lysis. Single-cell suspensions were filtered and washed with 10% RPMI solution.

Staining. Single-cell suspensions of cells resulting from tissue dissociations were stained (at 1:300 dilution unless otherwise stated) with different panels of antibodies with surface markers for CD45, CD4, CD8α, CD8β, TCRβ, TCRδ, NK1.1, Ly49, CD103, Thy1, PD-1, CD122, CD5, CD69, CD44, CD62L, CD38, CD244, CD3, CD31 (1:250 dilution), Ter-119 (1:250 dilution), CD49f (1:250 dilution), EpCAM (1:250 dilution), CD160 and Zombie UV Fixable Viability (1:1,000 dilution) and intracellular markers for T-bet, Ki67 and Foxp3. For intracellular staining, cells were stained for surface markers and fixed in eBioscience Fix/Perm buffer overnight, followed by permeabilization in eBioscience permeabilization buffer at room temperature for 45 min in the presence of antibodies. Cells were acquired with a BD LSRII or BD FACSymphony A3 via the FacsDiva v.8 program and analysis was performed with FlowJo v.10 software. All antibodies and staining reagents used in the study are outlined in Supplementary Tables 2 and 3.

Photoconversion procedure

Kaede transgenic mice were anesthetized, abdomen was surgically opened and a portion (approximately one-third in nonpregnant mice and a smaller portion in pregnant mice) of the small intestine was exposed. The mouse, except for the small intestine, was covered in aluminum foil and the small intestine was exposed to a handheld 405 nm blue purple laser for 30-s light pulses (which converts Kaede green cells to Kaede red cells). After photoconversion the mouse was surgically closed and killed 24 h later for flow cytometry analysis of Kaede green versus Kaede red cells.

Single-cell RNA and TCR sequencing

Mammary immunocytes. Live CD45$^+$ cells were sorted from the mammary gland of nulliparous ($n = 6$), gestation day 17 ($n = 4$), lactation day 3–5 ($n = 6$) and involution ($n = 4$) mice using a BD FACSAria after hashtagging with BioLegend TotalSeq-A reagents, and samples were pooled for encapsulation (10x Chromium). Libraries were prepared using Chromium Single-cell 3′ reagents kit v2 and sequenced on NovaSeq 6000.

Multi-organ combined scRNA-seq and TCR-seq. Live T cells (DAPI$^-$CD3$^+$CD44$^+$TCRβ$^+$) were sorted from the mammary gland, small intestines, large intestines, spleen and thymus from nulliparous ($n = 4$) and lactation day 4 ($n = 4$) mice. The cells were hashtagged with BioLegend TotalSeq-C reagents and pooled for encapsulation (10x Chromium). Libraries were prepared using Chromium Single-cell 5′ reagents kit v3 and sequenced on NovaSeq 6000. TCR and hashtag libraries were processed as described[29]. Hashtags used in the study can be found in Supplementary Table 3.

GF versus SPF. Live T cells (DAPI$^-$CD3$^+$CD44$^+$TCRβ$^+$) were sorted from GF ($n = 4$) and SPF ($n = 4$) mammary glands on lactation day 4. Samples were pooled for encapsulation (10x Chromium), libraries were prepared using Chromium Single-cell 3′ reagents kit v3 and sequenced on NovaSeq 6000.

Epithelial–IEL interactions. Live EpCAM$^+$CD45$^-$, CD45$^+$EpCAM$^-$ cells and TCRβ$^+$ cells were sorted from nulliparous and lactating mice, pooled for encapsulation (10x Chromium), libraries prepared using Chromium Single-cell 3′ reagents kit v3 and sequenced on NovaSeq 6000.

The scRNA-seq data were analyzed using the Seurat pipeline, which allowed for data normalization, clustering and identification of differentially expressed genes across groups.

Cell interaction predictions

CellChat v.2 was used to infer and visualize intercellular communication networks in the mammary gland[40,57]. CellChat v.2 is an R package that is able to predict and analyze intercellular communication pathways from single-cell data. The analysis was conducted as described in the CellChat v.2 published protocol. CellChat uses a manually curated database (CellChatDB) of literature-supported ligand–receptor signaling pathways, including multisubunit structures, cofactors, coreceptors, agonists and antagonists. Each potential interaction is assigned an interaction probability score based on the law of mass action to model the likelihood of an interaction based on the expression of the ligand, receptor and any cofactors. Statistically significant interactions are identified through a permutation test on randomly assigned group labels for cells.

In brief, EpCAM$^+$ and TCRβ$^+$ cells were isolated from the scRNA-seq data and used to predict intercellular communication pathways. We first identified differentially expressed genes ($P < 0.05$) between nulliparous and lactating mice for each cell population, and then mapped their projected interactions based on the fold change of ligands and receptors. For visualization purposes, the networks between EpCAM$^+$

and TCRβ$^+$ cells were isolated and visualized using chord diagrams. Summaries of signaling pathways were generated using CellChat v.2 and visualized using chord diagrams.

Histology, imaging and microscopy

Mouse mammary gland 4 was collected from nulliparous, gestation (G17), lactation (L3–5) and involution (I) stages and fixed in 4% paraformaldehyde (PFA) solution in PBS overnight at 4 °C with shaking. Mammary glands were washed with PBS and stored in 70% ethanol before being embedded in paraffin. Immunofluorescence staining was performed as previously described[58]. All primary antibodies were diluted in Renaissance Background reducing diluent (Biocare, PD905L). All opals were diluted 1:500 in 1× Plus Manual Amplification Diluent (Akoya Biosciences, FP1498).

Microscopy methods are reported following the guidance of Montero Llopis et al.[59] for best reproducible practices. Images in Fig. 2e and Extended Data Fig. 5d were acquired using an Olympus VS200 Slide Scanner widefield microscope equipped with a NOCEM X-cite light source (405–780 nm) and the fluorescent camera Hamamatsu Orca fusion BTsCMOS (2,304 × 2,304 pixels, 6.5 µm). Images were acquired using a UPlan X Apo ×20/0.8 air objective. Signal from DAPI, FITC, TRITC, CY5 and CY7 was collected by illuminating the sample using the FF409/493/573/652-Di02 or FF757-Di01 multiband dichroics and the following excitation (FF01-378/52, FF01-474/27, FF01-554/23, FF01-635/18 and FF01-735/28) and emission (FF01-432/36, FF01-515/30, FF01-595/31, FF01-698/70 and FF02-809/81) filters, respectively. Images were acquired using the OlyVIA v.2.9 software from Olympus and processed by Qpath and Fiji v.2.3 to crop representative areas and threshold background signal.

For H&E staining, sections were deparaffinized, stained with H&E, dehydrated and mounted with coverslips and imaged on an Olympus upright brightfield microscope at ×10 and ×20 magnification.

Milk alevoli quantification. Milk duct area was measured using Fiji v.2.3 to measure each duct in four different ×20 magnification images per mouse and the average of all ducts was calculated.

Human milk

Human milk samples (5ml each) were obtained from individual donors through the UCSD Human Milk Research Biorepository, and diluted 1:1 with PBS. Milk samples were centrifuged to remove lipid and whey layers. Remaining cells were stained using viability dye, CD4, CD94, CD8β, CD3, TCRδ, CD44, CD45, CD8α, CD103 and NKG2D. Antibodies used in the study are listed in Supplementary Table 2. Cells were analyzed using BD LSRFortessa or BD FACSymphony A3 via the FacsDiva v.8 program and analysis was performed with FlowJo v.10 software. The protocol for analysis of human milk samples was approved by the UCSD Institutional Review Board Administration (no. 808920) and patients provided written informed consent before enrollment.

Quantification and statistical analysis

Data are presented as mean ± s.e.m. Unless stated otherwise, significance was assessed by a Student's *t*-test in GraphPad Prism v.8.0.

Reporting summary

Further information on research design is available in the Nature Portfolio Reporting Summary linked to this article.

Data availability

The scRNA-seq and TCR-seq data are available in the National Center for Biotechnology Information under accession nos. GSE290256 and GSE288901. Mammary gland T cell data are available in a user-friendly format at https://cbdm.connect.hms.harvard.edu/ImmgenT/PublicRosetta/.

References

55. Tomura, M. et al. Monitoring cellular movement in vivo with photoconvertible fluorescence protein 'Kaede' transgenic mice. *Proc. Natl Acad. Sci. USA* **105**, 10871–10876 (2008).
56. Morton, A. M. et al. Endoscopic photoconversion reveals unexpectedly broad leukocyte trafficking to and from the gut. *Proc. Natl Acad. Sci. USA* **111**, 6696–6701 (2014).
57. Jin, S., Plikus, M. V. & Nie, Q. CellChat for systematic analysis of cell-cell communication from single-cell transcriptomics. *Nat. Protoc.* **20**, 180–219 (2025).
58. Sorrelle, N. et al. Improved multiplex immunohistochemistry for immune microenvironment evaluation of mouse formalin-fixed, paraffin-embedded tissues. *J. Immunol.* **202**, 292–299 (2019).
59. Montero Llopis, P. et al. Best practices and tools for reporting reproducible fluorescence microscopy methods. *Nat. Methods* **18**, 1463–1476 (2021).

Acknowledgements

We thank G. Ascui-Gac and M. Kronenburg for reagents and advice on MAIT cell analysis and Q. Vallmajo Martin, D. Umar and A. Quach for helpful discussions. This work was supported by a Damon Runyon Dale F. Frey Award to D.R., National Institutes of Health (NIH) grants RO1-AI150686 to C.B.; R24-072073 to the ImmGen Consortium; University of California, San Diego, Pathway in Biological Sciences T32 GM133351 to A.J., NIH–National Cancer Institute (NCI) CCSG P30 CA014195, NIH–National Institute on Aging San Diego Nathan Shock Center P30 AG068635, the Chapman Foundation and the Helmsley Charitable Trust to the Next-Generation Sequencing Core Facility of the Salk Institute (RRID:SCR_014846 and SCR_026396); and NIH–NCI CCSG: P30 CA01495, and Shared Instrumentation Grants S10-OD023689 (Aria Fusion cell sorter) and S10 OD034268 (Thermo Fisher Bigfoot) to the Flow Cytometry Core Facility of the Salk Institute (RRID:SCR_014839).

Author contributions

Conception and design: A.J., C.B. and D.R. Experimentation: A.J., E.P., P.B., S.G.-P., I.M., I.B. and E.M. Computation: E.P., X.G., P.B., A.R.M.-R. and C.B. Data interpretation: A.J., P.B., A.R.M.-R., J.A., D.M., C.B. and D.R. Human samples: K.B. and C.C. Writing – original draft: A.J., C.B. and D.R. Writing – review and editing: all authors.

Competing interests

The authors declare no competing interests.

Additional information

Extended data is available for this paper at https://doi.org/10.1038/s41590-025-02218-3.

Supplementary information The online version contains supplementary material available at https://doi.org/10.1038/s41590-025-02218-3.

Correspondence and requests for materials should be addressed to Deepshika Ramanan.

Peer review information *Nature Immunology* thanks Mahima Swamy, Luc Van Kaer and the other, anonymous, reviewer(s) for their contribution to the peer review of this work. Primary Handling Editor: S. Houston in collaboration with the *Nature Immunology* team.

https://doi.org/10.1038/s41590-025-02218-3

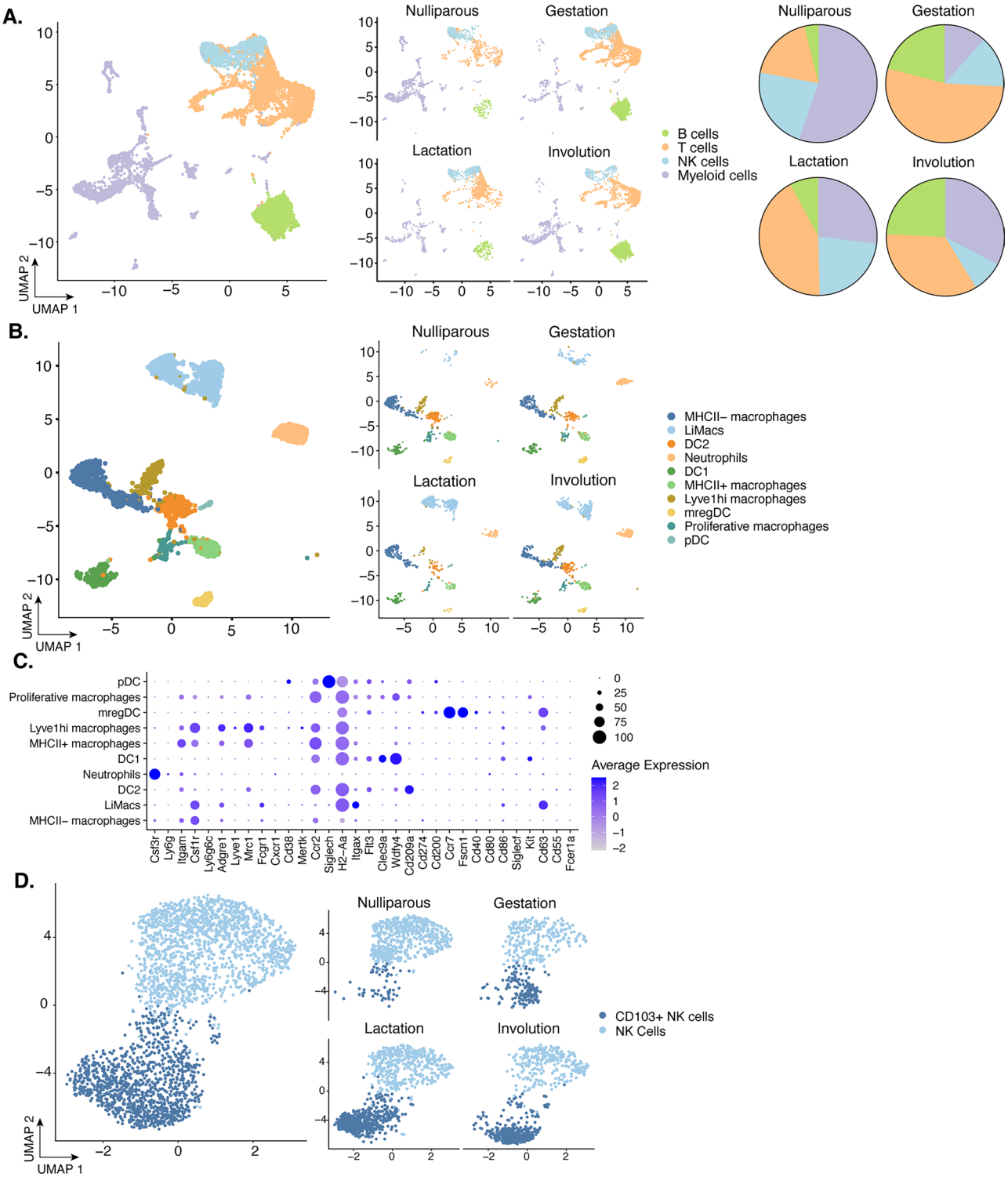

Extended Data Fig. 1 | Myeloid populations in the mammary gland during gestation and lactation. a) UMAP projection of all immunocytes in the mammary gland (left) split by stages nulliparous, gestation (G17), lactation (L3), and involution (right). Pie charts summarizing the proportions of cell populations in each stage (far right). **b**) UMAP projection of all myeloid cells in the mammary gland (left) split by stages nulliparous, gestation (G17), lactation (L3), and involution (right). **c**) Dot plot of myeloid cell population markers. Dot size represents the percentage of cells expressing the selected gene and color indicates expression level. **d**) UMAP projection of NK cell populations in the mammary gland (left) split by stages nulliparous, gestation (G17), lactation (L3), and involution (right). Data representative of 3 independent experiments.

https://doi.org/10.1038/s41590-025-02218-3

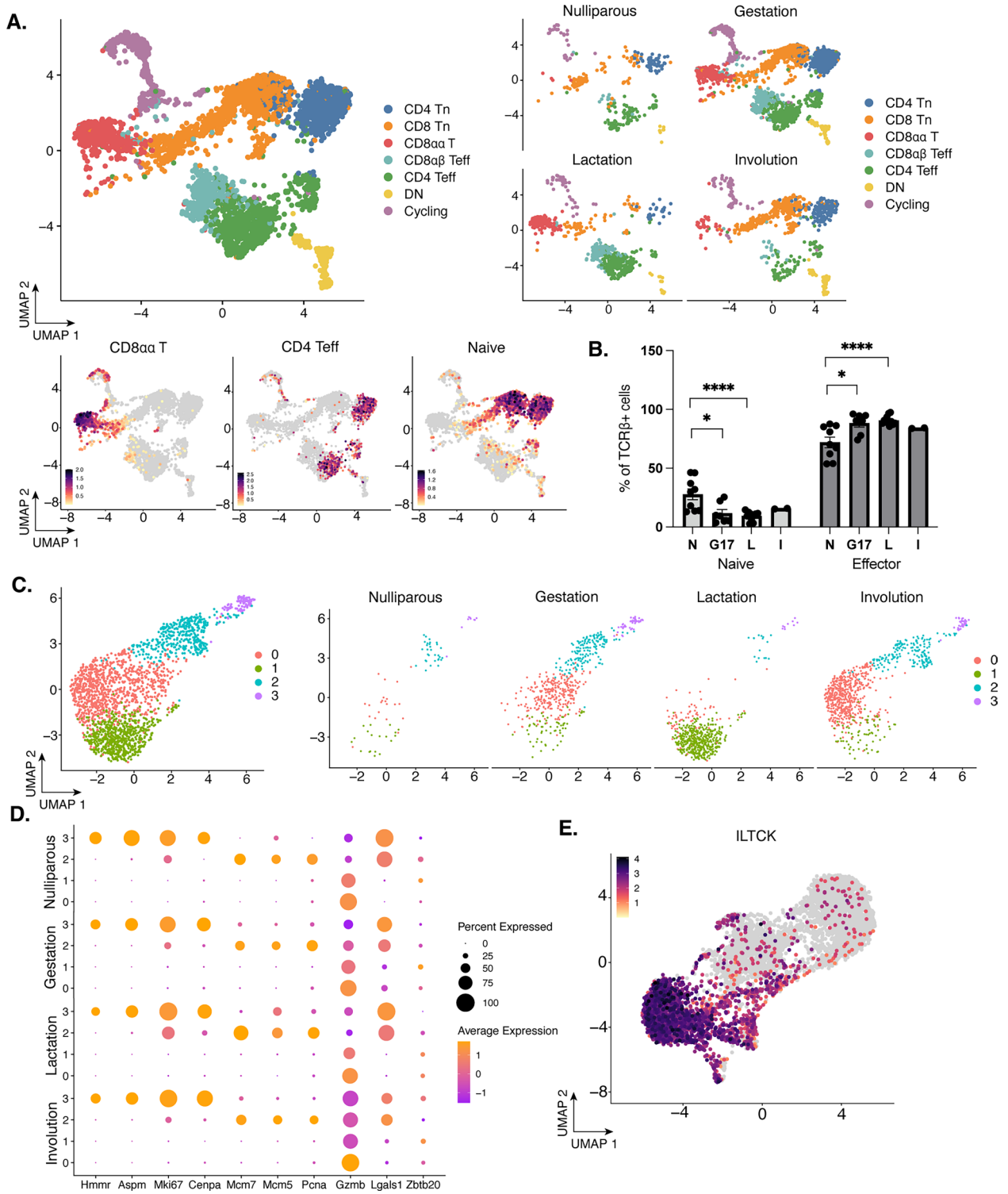

Extended Data Fig. 2 | T cell changes in the lactating mammary gland are reproducible across mice and experiments. a) UMAP projection of mammary T cells with feature plots of specified T cell gene signatures (left). Split by stages: nulliparous, gestation (G17), lactation (L3), and involution (right). **b**) Quantification of the proportion of CD44+ (effector) and CD44- (naive) T cells across stages. N=nulliparous (n = 9), G17=gestation day 17 (n = 7), L=lactation days 3–5 (n = 11) and I=involution, 1 day post-weaning (n = 2). **c**) UMAP projection of CD8αα+ cell populations (left) split by stages nulliparous, gestation (G17), lactation (L3), and involution (right). **d**) Dot plot of selected highly upregulated genes for CD8αα+ populations across stages identified in (**c**). Dot size represents the percentage of cells expressing the selected gene and color indicates expression level. **e**) UMAP projection of the ILTCK gene signature (Chou et al.[32]) on the summary T cell UMAP from Fig. 1c. Two tailed unpaired Student's t-tests were performed on the results shown in **b**. *p < 0.05, ****p < 0.0001. Data representative of ≥3 independent experiments, bars in plots indicate mean ± SEM.

https://doi.org/10.1038/s41590-025-02218-3

Extended Data Fig. 3 | Differential gene expression in T cell populations across stages. a) Heatmaps of top differentially expressed genes in specified T cell populations across nulliparous, gestation, lactation and involution stages. Data is representative of 3 independent experiments.

https://doi.org/10.1038/s41590-025-02218-3

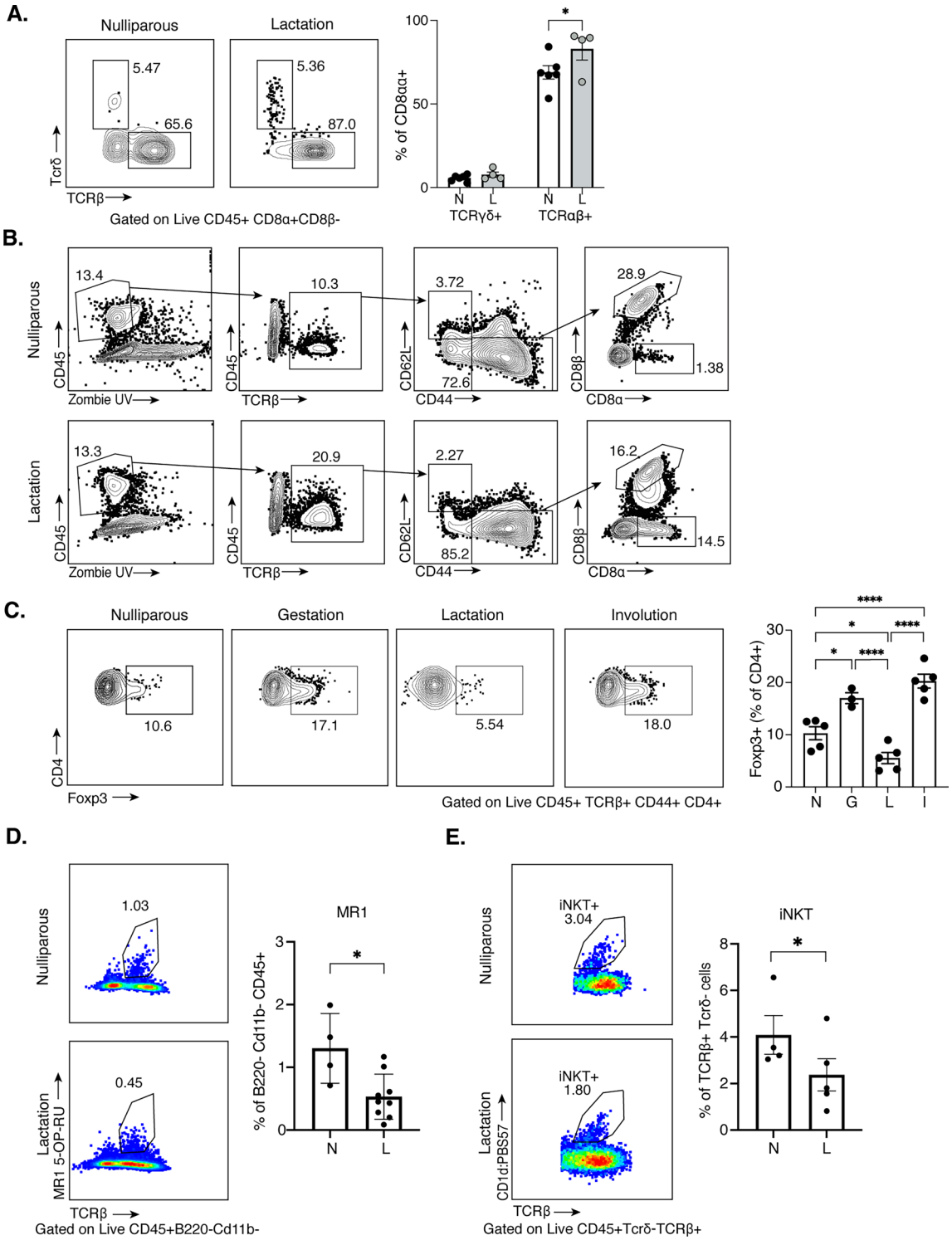

Extended Data Fig. 4 | Unconventional T cell subsets are a minor population in the mammary gland. a) Representative flow cytometry plots and quantification indicating the proportion of mammary CD8αα+ cells that are TCRδ + and TCRβ+ in N=nulliparous (n = 6) and L=lactation days 3–5 (n = 4) mice. **b**) Representative gating for flow cytometry analysis with final gating on the CD8αα+ and CD8αβ+ mammary populations in nulliparous and lactation. **c**) Representative flow cytometry plots and proportion of mammary Foxp3+ T regulatory cells in N=nulliparous (n = 5), G=gestation day 17 (n = 3), L=lactation days 3–5 (n = 5) and I=involution, 1 day post-weaning (n = 5). **d**) Representative flow cytometry plots and proportion of mammary MR1 5-OP-RU + T cells of CD45 + B220- Cd11b- cells in N=nulliparous (n = 4) and L=lactation days 3–5 (n = 9) mice. **e**) Representative flow cytometry plots and proportion of mammary iNKT+ cells of all CD45 + TCRβ+ cells in N=nulliparous (n = 4) and L=lactation days 3–5 (n = 5) mice. Two tailed unpaired Student's t-tests were performed on the results shown in **a, c, d** and **e**.*p < 0.05, ****p < 0.0001. Data representative of ≥3 independent experiments, bars in plots indicate mean ± SEM.

https://doi.org/10.1038/s41590-025-02218-3

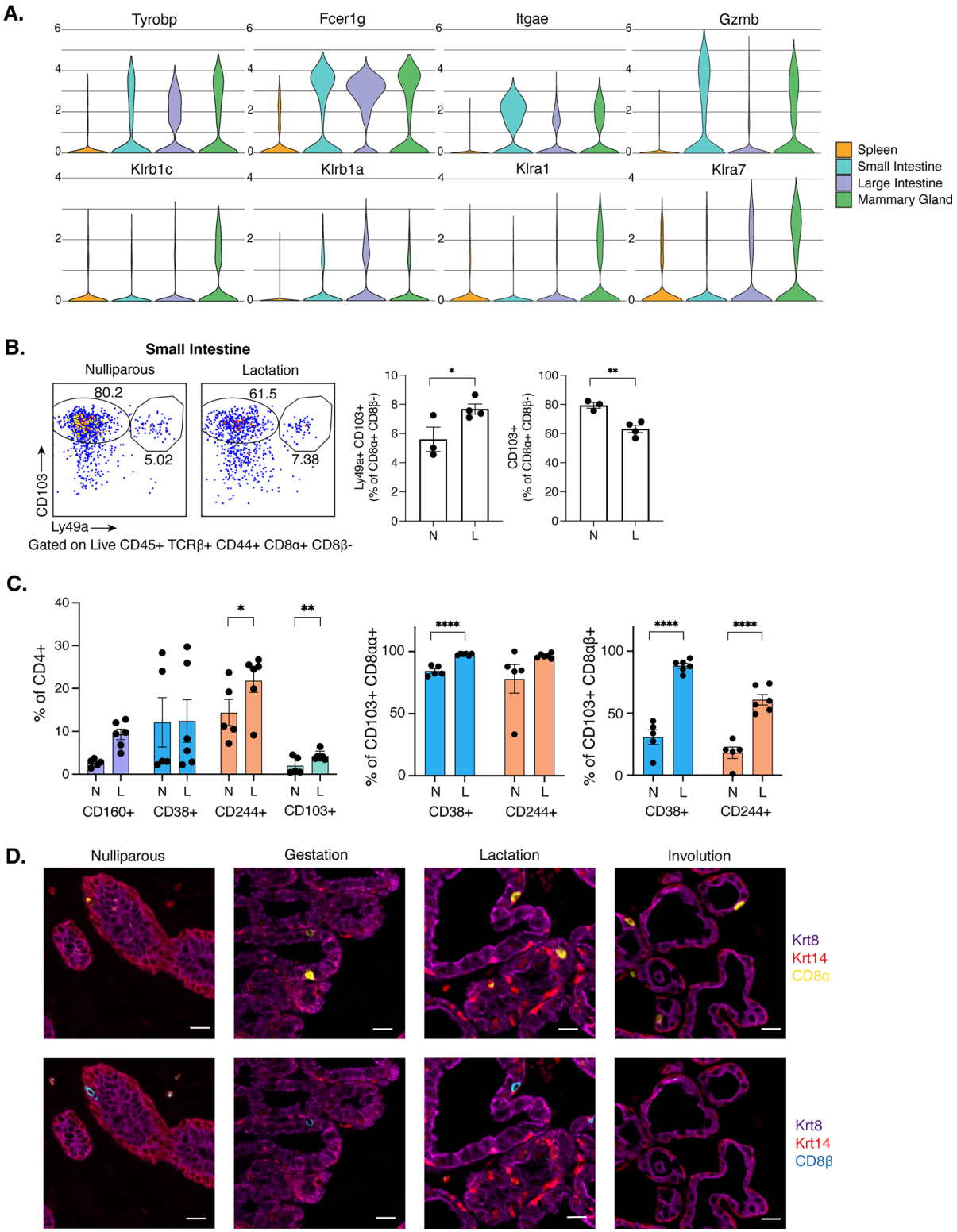

Extended Data Fig. 5 | Mammary T cells display similar markers to intestinal T cells and are intraepithelial in location. a) Violin plots depicting gene expression of classical IEL markers in CD8 + T cells from spleen, small intestinal epithelium, large intestinal epithelium and mammary gland of lactating mice. **b**) Representative flow cytometry plots and proportion of CD103+ and CD103 + Ly49+ cells in the CD8αα+ population in the small intestine in N=nulliparous (n = 3) and L=lactation days 3–5 (n = 4). **c**) Proportion of CD4+ cells that express CD160, CD38, CD244, and CD103 in N=nulliparous (n = 5) and L=lactation days 3–5 (n = 6) (left). Proportion of CD103+ cells that are CD38+ and CD244+ in CD8αα+ and CD8αβ + T cell subsets in nulliparous (n = 5) and lactation (n = 6) (right). **d**) Representative immunofluorescence images of the mammary gland at nulliparous, gestation (G17), lactation (L3), and involution of the epithelium (Krt8, luminal cells, in magenta and Krt14, basal cells, in red), and T cell markers, CD8α (yellow), CD8β (cyan). Images match Fig. 2e (top) to show the overlap of cells positive for CD8α and CD8β within the epithelial layer. Scale bar = 20μm. Two tailed unpaired Student's t-tests were performed on the results shown in **b** and **c**.*$p < 0.05$, **$p < 0.01$, ****$p < 0.0001$. Data representative of ≥3 independent experiments for imaging and flow cytometry, bars in plots indicate mean ± SEM. 2 independent experiments for scRNAseq.

https://doi.org/10.1038/s41590-025-02218-3

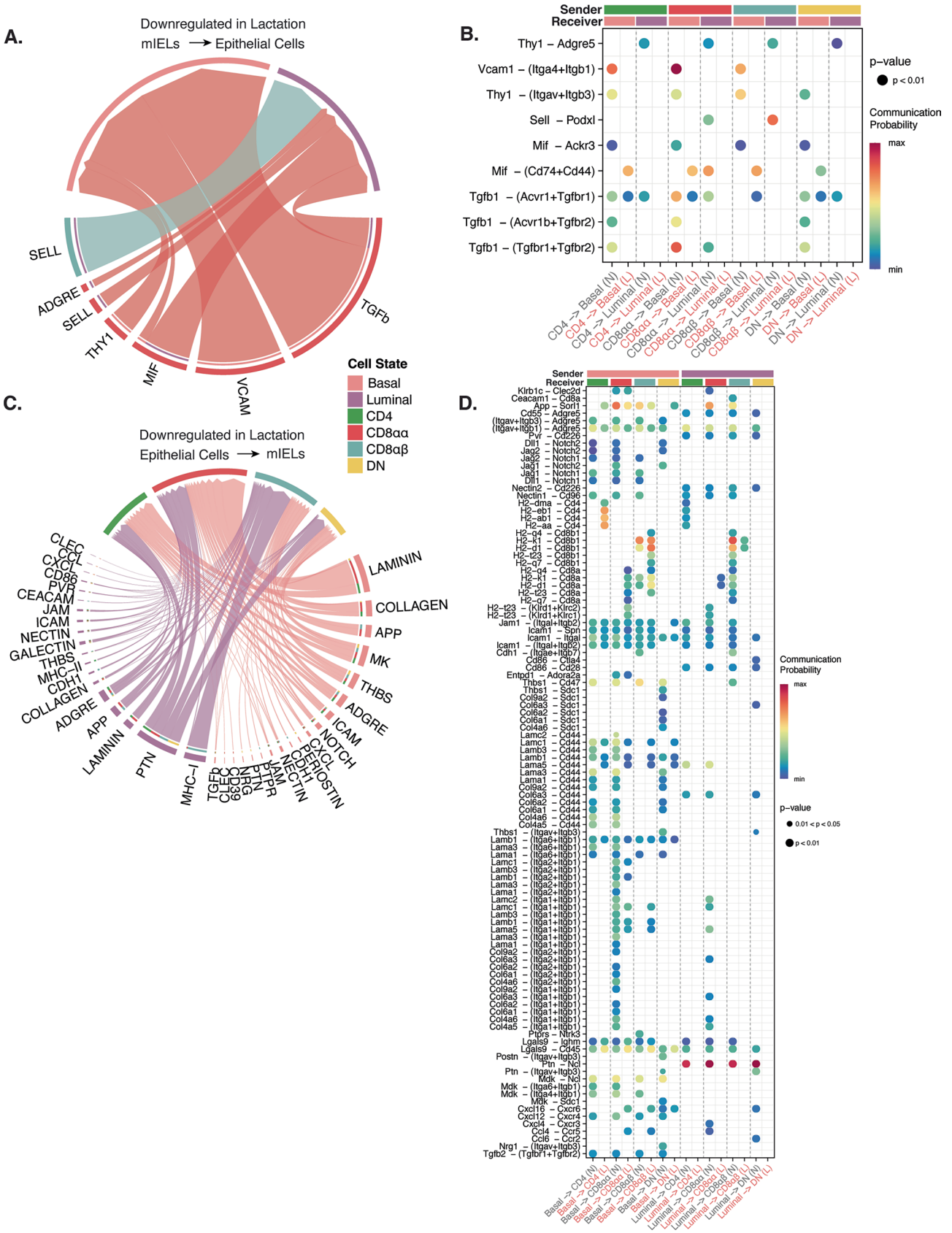

Extended Data Fig. 6 | See next page for caption.

https://doi.org/10.1038/s41590-025-02218-3

Extended Data Fig. 6 | Putative interaction networks between mIELs and epithelial cells downregulated during lactation. a, c) Chord diagrams showing potential signaling pathways downregulated in lactation from mIEL populations to epithelial cells (**a**) and from epithelial cells to mIEL populations (**c**). Ligand:receptor pairs as summarized into functionally related signaling pathways. Outer thicker bars represent the cell population that is the source or target of the signaling pathway in the chord diagram. The inner thinner bar color is the target of the signal. The thickness of the edge represents the signaling strength (communication probability) as calculated by CellChat. **b, d**) Dot plots showing the communication probabilities of ligand:receptor pairs downregulated in lactation from mIELs to epithelial cells (**b**) and from epithelial cells to mIEL populations (**d**). Heatmap depicts the communication probability of each ligand:pair for each cell pair in nulliparous (N) and lactating (L) mammary glands. Sender and receivers are indicated by the color bars on top. P-value's computed by CellChatv2 from a one-sided permutation test. Data generated using scRNAseq of epithelial and mIEL populations in nulliparous (n = 2) and lactating (n = 2) mammary glands. P-values are computed by CellChatv2 from a one-sided permutation test.

https://doi.org/10.1038/s41590-025-02218-3

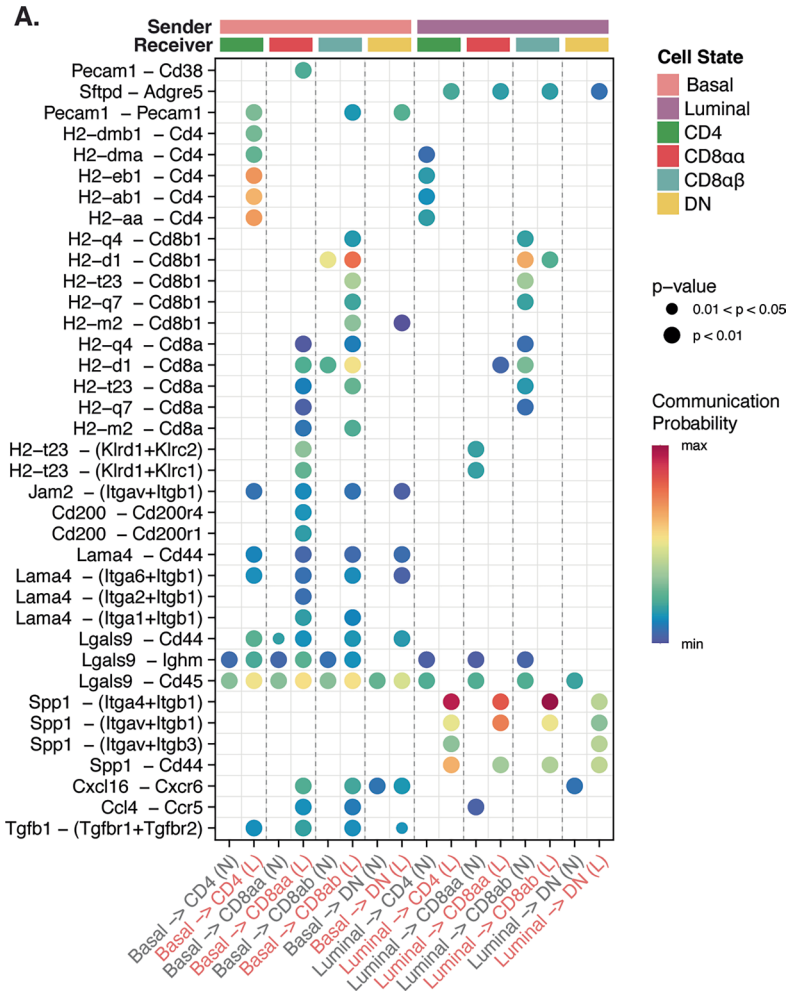

Extended Data Fig. 7 | Putative ligand:receptor pairs from epithelial cells to mIELs upregulated during lactation. a) Dot plot showing the communication probabilities of ligand:receptor pairs upregulated in lactation from epithelial cells to mIEL populations. Heatmap depicts the communication probability of each ligand:pair for each cell pair in nulliparous (N) and lactating (L) mammary glands. Sender and receivers are indicated by the color bars on top. P-value's computed by CellChatv2 from a one-sided permutation test. Data generated using scRNAseq of epithelial and mIEL populations in nulliparous (n = 2) and lactating (n = 2) mammary glands. P-values are computed by CellChatv2 from a one-sided permutation test.

https://doi.org/10.1038/s41590-025-02218-3

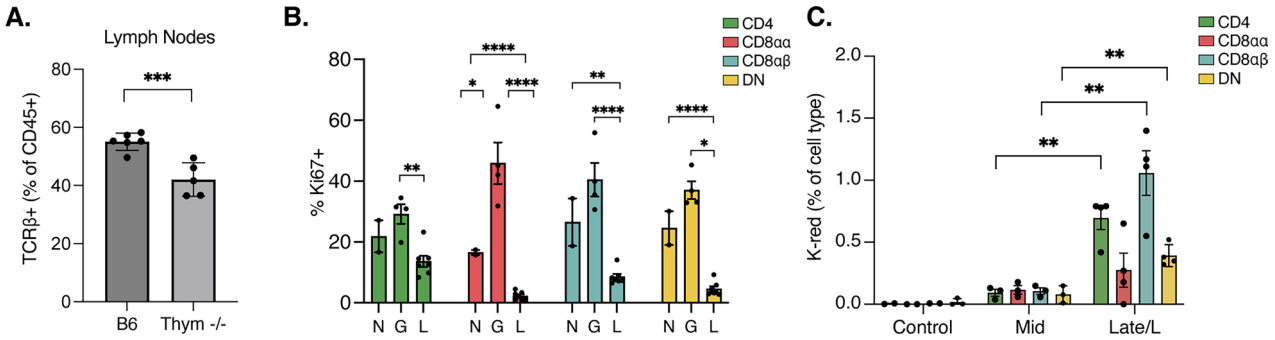

Extended Data Fig. 8 | Thymic vs intestinal input in mIEL expansion. **a**) Quantification of the proportion of TCRβ+ cells (of CD45 +) in B6 (n = 6) and thymectomized lactating (n = 5) (L3–5) mammary gland lymph nodes. **b**) Proportion of mIEL populations in the mammary gland that are Ki67 + . N=nulliparous (n = 2), G=gestation day 17 (n = 4), and L=lactation days 3–5 (n = 7). mIEL populations were determined as CD4: CD4 + CD44 + CD62L-. CD8αα: CD8α + CD8β-CD44 + CD62L-. CD8αβ: CD8α + CD8β + CD44 + CD62L-. DN: TCRβ + CD4-CD8α-. **c**) Proportion of Kaede red cells within T cell populations (gated on TCRβ+ followed by either CD4 + , CD8β + , CD8α + CD8β-, or DN) in the spleen 24 hours post-photoconversion of the intestine. Controls are non-photoconverted mice (n = 3), mid being mice photoconverted on gestation day 10 and analyzed on gestation day 11 (n = 3) and late/L representing mice both photoconverted on gestation day 16 and analyzed on gestation day 17 and mice photoconverted on lactation day 1 and analyzed on lactation day 2 (n = 4). Two tailed unpaired Student's t-tests were performed on the results shown in **a, b** and **c**.*p < 0.05, **p < 0.01, ***p < 0.001, ****p < 0.0001. Data representative of ≥3 independent experiments for flow cytometry and Kaede experiments, bars in plots indicate mean ± SEM.

https://doi.org/10.1038/s41590-025-02218-3

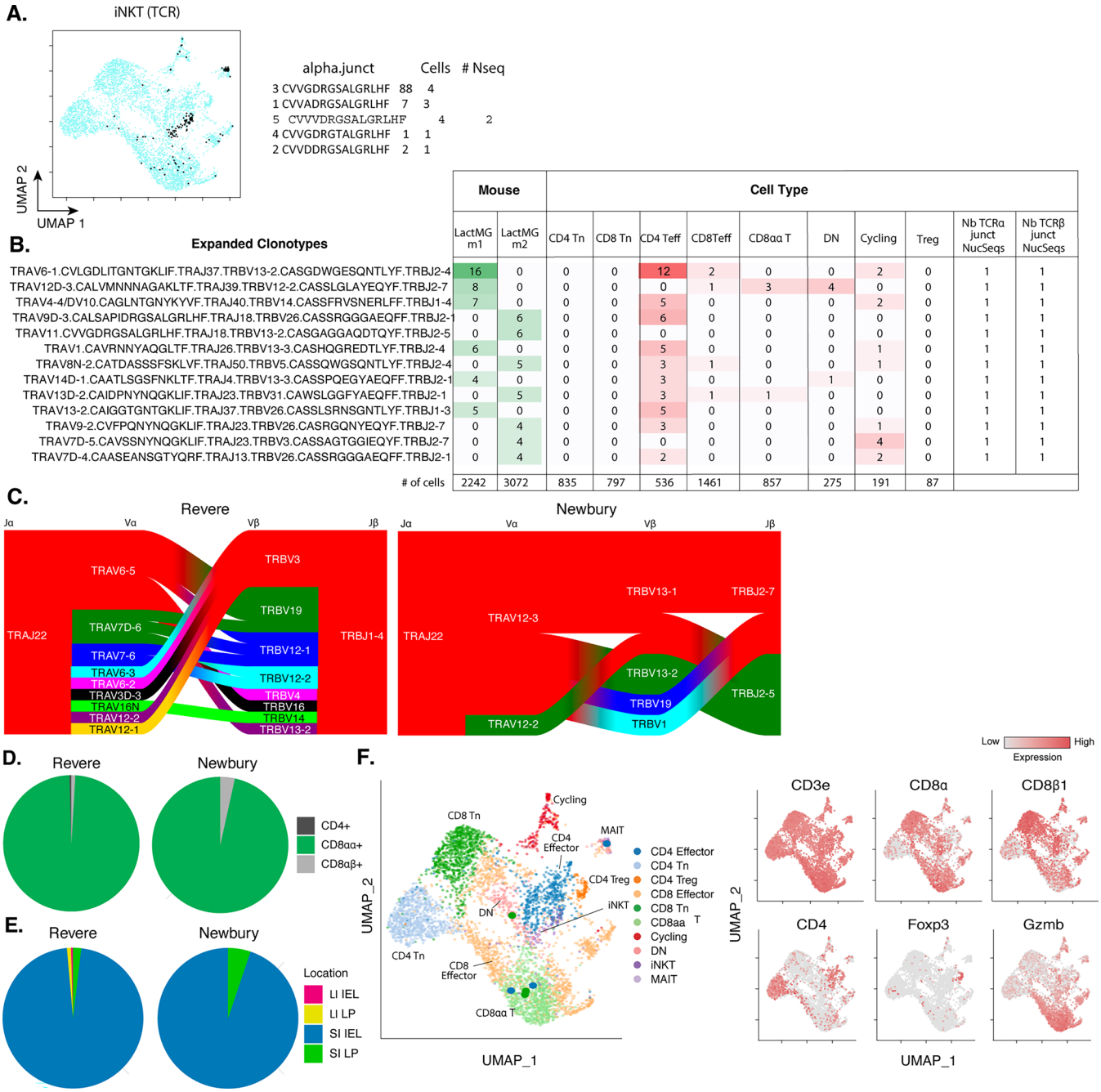

Extended Data Fig. 9 | TCR clonotypes expand across different T cell types, and Revere and Newbury TCRs are only expressed in CD8αα + mIELs and iIELs. a) UMAP and quantification of cells with different alpha junction usage. **b**) Quantification of expanded clonotypes across mice and cell types. **c**) V region usage of Revere and Newbury TCR families. **d**) Quantification of Revere and Newbury families in different IEL populations in the small intestine. **e**) Quantification of Revere and Newbury families in the IEL and lamina propria compartments in the small intestine and large intestine. **f**) UMAP projection of lactating mammary gland T cells with highlighted dots representing cells expressing Revere and Newbury TCRs (left) with feature plots of T cell genes (right). Data representative of ≥2 independent experiments.

https://doi.org/10.1038/s41590-025-02218-3

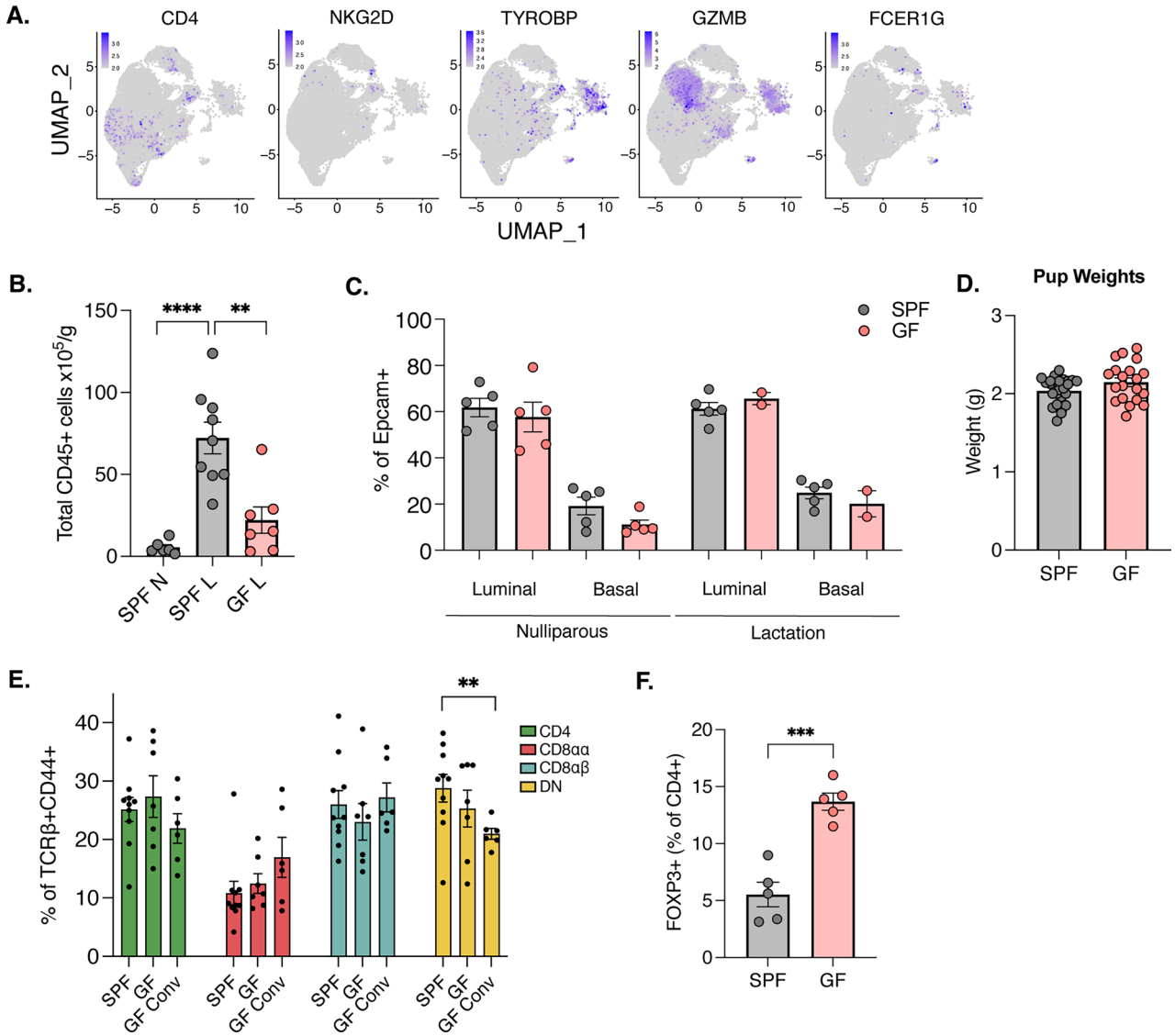

Extended Data Fig. 10 | Characterization of human mIEL-like cells and lactogenesis in germ-free mice. a) Feature plots of select CD8αα + T markers, cytotoxic markers and tissue resident genes projected on UMAP from human breast tissue (6A). **b**) Quantification of total number of CD45+ cells normalized to mammary gland weight in nulliparous and lactating SPF and GF lactating mice. **c**) Proportion of basal (Epcam int (intermediate) and CD49f high) and luminal (Epcam high and CD49f low) cells in SPF (n = 5) and GF (n = 5 nulliparous and n = 2 lactating) nulliparous and lactating mammary glands. Taken as a percentage of all Epcam+ cells. **d**) The weight (grams) of pups from GF (n = 3 litters) and SPF (n = 4 litters) litters at 4 days of birth normalized to litter size. **e**) mIEL proportions of TCRβ + CD44+ cells of SPF (n = 10), GF (n = 7), and GF conventionalized (n = 6) mammary glands. mIEL populations were determined as CD4: CD4 + CD44 + CD62L-. CD8αα: CD8α + CD8β-CD44 + CD62L-. CD8αβ: CD8α + CD8β + CD44 + CD62L-. DN: TCRβ + CD4-CD8α-. **f**) Proportion of mammary Foxp3+ T regulatory cells in lactating SPF (n = 5) and GF mice (n = 5). Two tailed unpaired Student's t-tests were performed on the results shown in **b**, **c**, **d**, **e** and **f**. **p < 0.01, ***p < 0.001, ****p < 0.0001. Data representative of ≥ 3 independent experiments, bars in plots indicate mean ± SEM.

nature portfolio

Corresponding author(s): Deepshika Ramanan

Last updated by author(s): Jun 6, 2025

Reporting Summary

Nature Portfolio wishes to improve the reproducibility of the work that we publish. This form provides structure for consistency and transparency in reporting. For further information on Nature Portfolio policies, see our Editorial Policies and the Editorial Policy Checklist.

Statistics

For all statistical analyses, confirm that the following items are present in the figure legend, table legend, main text, or Methods section.

n/a	Confirmed	
☐	☒	The exact sample size (*n*) for each experimental group/condition, given as a discrete number and unit of measurement
☐	☒	A statement on whether measurements were taken from distinct samples or whether the same sample was measured repeatedly
☐	☒	The statistical test(s) used AND whether they are one- or two-sided *Only common tests should be described solely by name; describe more complex techniques in the Methods section.*
☐	☒	A description of all covariates tested
☐	☒	A description of any assumptions or corrections, such as tests of normality and adjustment for multiple comparisons
☐	☒	A full description of the statistical parameters including central tendency (e.g. means) or other basic estimates (e.g. regression coefficient) AND variation (e.g. standard deviation) or associated estimates of uncertainty (e.g. confidence intervals)
☐	☒	For null hypothesis testing, the test statistic (e.g. *F*, *t*, *r*) with confidence intervals, effect sizes, degrees of freedom and *P* value noted *Give P values as exact values whenever suitable.*
☒	☐	For Bayesian analysis, information on the choice of priors and Markov chain Monte Carlo settings
☐	☒	For hierarchical and complex designs, identification of the appropriate level for tests and full reporting of outcomes
☒	☐	Estimates of effect sizes (e.g. Cohen's *d*, Pearson's *r*), indicating how they were calculated

Our web collection on statistics for biologists contains articles on many of the points above.

Software and code

Policy information about availability of computer code

Data collection	Images were acquired using the OlyVIA 2.9 software from Olympus. Flow cytometry data were acquired using BD FacsDiva 8 software. RNA sequencing was performed on Illumina NovaSeq 6000.
Data analysis	Images were processed by Qpath and FIJI 2.3 to crop representative areas and threshold background signal. Flow cytometry analysis was performed with FlowJo 10 software. Single-cell RNAseq data was analyzed using the Seurat pipeline by the Satija Lab, which allowed for data normalization, clustering, and identification of differentially expressed genes across groups. Summary of signaling pathways were generated using CellChat v2. GraphPad Prism v8.0 used for analysis and graph building.

For manuscripts utilizing custom algorithms or software that are central to the research but not yet described in published literature, software must be made available to editors and reviewers. We strongly encourage code deposition in a community repository (e.g. GitHub). See the Nature Portfolio guidelines for submitting code & software for further information.

Data

Policy information about availability of data

All manuscripts must include a data availability statement. This statement should provide the following information, where applicable:

- Accession codes, unique identifiers, or web links for publicly available datasets
- A description of any restrictions on data availability
- For clinical datasets or third party data, please ensure that the statement adheres to our policy

Single cell sequencing data are available in NCBI with accession numbers GSE290256 and GSE288901. Mammary gland T cell data are available in a user-friendly format at
https://cbdm.connect.hms.harvard.edu/ImmgenT/PublicRosetta/

Research involving human participants, their data, or biological material

Policy information about studies with human participants or human data. See also policy information about sex, gender (identity/presentation), and sexual orientation and race, ethnicity and racism.

Reporting on sex and gender	In this study, milk samples were collected exclusively from postpartum women, as the focus was on analyzing milk composition during lactation. Since only women can produce milk postpartum, male participants were not included. This decision was made to ensure that the sample population was relevant to the study's objectives, specifically examining female lactation.
Reporting on race, ethnicity, or other socially relevant groupings	We did not use population characteristics in our data analysis.
Population characteristics	We did not use population characteristics in our data analysis.
Recruitment	Participants were recruited under completely voluntary circumstances, with individuals donating milk samples to the milk bank at UCSD. Since the recruitment process was entirely voluntary, there was no self-bias introduced, as the participants were simply those willing to contribute to the milk bank.
Ethics oversight	University of California San Diego Institutional Review Board Administration

Note that full information on the approval of the study protocol must also be provided in the manuscript.

Field-specific reporting

Please select the one below that is the best fit for your research. If you are not sure, read the appropriate sections before making your selection.

☒ Life sciences ☐ Behavioural & social sciences ☐ Ecological, evolutionary & environmental sciences

For a reference copy of the document with all sections, see nature.com/documents/nr-reporting-summary-flat.pdf

Life sciences study design

All studies must disclose on these points even when the disclosure is negative.

Sample size	We determined the sample size based on a power analysis, aiming for sufficient power to detect meaningful differences. Given practical constraints and the nature of our study, we chose to include 3-5 mice per group per experiment, repeating each experiment at least 2 times in the case of sequencing or 3 or more times in the case of flow cytometry and imaging. This sample size was deemed appropriate to detect the expected effect size and statistical significance while minimizing animal use.
Data exclusions	No data were excluded
Replication	All flow cytometry (including Kaede, germ free and thymectomy mice) and imaging experiments were repeated at least three times and single cell RNAseq experiments were repeated at least two times. All attempts at replication were successful. 10 human milk sample were received and processed on individual days, sample preparation failed on 3 occasions and those samples were excluded from the reported data resulting in 7 successful repeated experiments.
Randomization	To account for natural variation in pregnancy and lactation in all mouse experiments, we randomized the assignment of litter mates to different experimental groups. Since we are studying different stages of pregnancy and lactation, litter mates were randomly assigned to the various groups at each stage. Human milk samples were received on a rolling basis, depending on the availability and willingness of donors, resulting in a random and unscheduled collection process.
Blinding	Blinding was not implemented in this study because the different stages of pregnancy are visibly distinguishable due to physical and behavioral changes in the animals. These visible differences make it impossible to blind the study without introducing confusion. However we

used objective, standardized outcome measures and studied different stages of pregnancy using litter mates to minimize bias and ensure reliable results, as litter mates share similar genetic backgrounds and environmental conditions. This applies to all mouse studies. The human samples were obtained through a clinical study and the researchers that processed the samples had no access to donor identities or their clinical information.

Reporting for specific materials, systems and methods

We require information from authors about some types of materials, experimental systems and methods used in many studies. Here, indicate whether each material, system or method listed is relevant to your study. If you are not sure if a list item applies to your research, read the appropriate section before selecting a response.

Materials & experimental systems

n/a	Involved in the study
☐	☒ Antibodies
☒	☐ Eukaryotic cell lines
☒	☐ Palaeontology and archaeology
☐	☒ Animals and other organisms
☒	☐ Clinical data
☒	☐ Dual use research of concern
☒	☐ Plants

Methods

n/a	Involved in the study
☒	☐ ChIP-seq
☐	☒ Flow cytometry
☒	☐ MRI-based neuroimaging

Antibodies

Antibodies used

Antibodies used for flow cytometry and sorting were used at 1:300 dilution unless otherwise indicated below:
anti-mouse CD45, BV510 (clone S18009F), 157219, Biolegend
anti-mouse TCRb, FITC (clone H57-597), 109206, Biolegend
anti-mouse CD8a, BV421/PB (clone 53-6.7), 100725, Biolegend
anti-mouse Ly49AB6, PE (clone A1/Ly49A), 138703, Biolegend
anti-mouse Ly49CFIH, PE (clone 14B11), 108208, Biolegend
anti-mouse CD8b, PerCP-Cy5.5 (clone YTS156.7.7), 126610, Biolegend
anti-mouse CD103, PE Cy7 (clone 2E7), 121426, Biolegend
anti-mouse NK1.1, APC-Cy7 (clone PK136), 108724,Biolegend
anti-mouse TCRgd, APC (clone GL3), 118116, Biolegend
anti-mouse CD4, AF700 (clone GK1.5) 100430, Biolegend
anti-mouse CD4, FITC (clone GK1.5), 100406, Biolegend
anti-mouse TCRb, PE (clone H57-597), 109208, Biolegend
anti-mouse Foxp3, PE-Cy7 (clone FJK-16s), 25-5773-82, Thermo Fisher Scientific
anti-mouse CD69, APC-Cy7 (clone H1.2F3), 104526, Biolegend
anti-mouse CD44, APC (clone IM7), 103012, Biolegend
anti-mouse CD62L, AF700 (clone MEL-14), 104426, Biolegend
anti-mouse CD103, AF700 (clone 2E7), 121441, Biolegend
anti-mouse CXCR6, APC-Cy7 (clone SA051D1), 151123, Biolegend
anti-mouse B220, PE-Cy7 (clone RA3-6B2), 103222, Biolegend
anti-mouse CD11b, PerCP-Cy5.5 (clone M1/70), 101228, Biolegend
anti-mouse CD11c, APC (clone N418), 117310, Biolegend
anti-mouse TCRgd, BV421/PB (clone GL3), 118120, Biolegend
anti-mouse Thy1, PE (clone 30-H12), 105307, Biolegend
anti-mouse CD4, PerCP-Cy5.5 (clone GK1.5), 100434, Biolegend
anti-mouse PD-1, PE-Cy7 (clone 29F.1A12), 135216, Biolegend
anti-mouse CD122, APC (clone TMβ1), 123213, Biolegend
anti-mouse CD5, AF700 (clone 53-7.3), 100636, Biolegend
anti-mouse CD8a, AF700 (clone 53-6.7), 100730, Biolegend
anti-mouse Ki67, PE-Cy7 (clone B56), 561283, BD Pharmigen
anti-mouse CD160, PE-Cy7 (clone 7H1), 143010, Biolegend
anti-mouse CD38, APC-Cy7 (clone 90), 102727, Biolegend
anti-mouse CD244, APC (clone m2B4 (B6)458.1), 133517, Biolegend
anti-mouse CD3, APC (clone 17A2), 100236, Biolegend
anti-mouse T-bet, PE-Dazzle594 (clone 4B10), 644828, Biolegend
Zombie UV, UV, 423108, Biolegend, used at a 1:1000 dilution.
anti-human CD4, FITC (clone RPA-T4), 300506, Biolegend
anti-human CD94, PerCP-Cy5.5 (clone DX22), 305514, Biolegend
anti-human CD8b, PE (clone QA20A40), 376703, Biolegend
anti-human TCRb, PE-Cy7 (clone IP26), 306719, Biolegend
anti-human TCRgd, APC (clone B1), 331211, Biolegend
anti-human/mouse CD44, APC-Cy7 (clone IM7), 103027, Biolegend
anti-human CD45, BV510 (clone HI30), 304035, Biolegend
anti-human CD8a, BV605 (clone RPA-T8), 301039, Biolegend
anti-human CD103, BV711 (clone Ber-ACT8), 350221, Biolegend
anti-human NKG2D, BV785 (clone 1D11), 320829, Biolegend

anti-mouse CD45, BV421/PB (clone30-F11), 103133, Biolegend
anti-mouse CD31, BV421/PB (clone 390), 102423, Biolegend, used at 1:250 dilution
anti-mouse Ter-119, BV421/PB (clone TER-119), 116233, Biolegend, used at 1:250 dilution
anti-mouse CD49f, APC-Cy7 (clone GoH3), 313627, Biolegend, used at 1:250 dilution
anti-mouse Ep-CAM, AF647 (clone G8.8), 118212, Biolegend, used at 1:250 dilution

Validation

All antibodies are from commercial sources and have been validated by the vendors. Validation data are available on the manufacturer's website.

Animals and other research organisms

Policy information about studies involving animals; ARRIVE guidelines recommended for reporting animal research, and Sex and Gender in Research

Laboratory animals

C57BL/6 (B6) mice were purchased from Jackson Labs and maintained in specific pathogen free (SPF) conditions at Harvard Medical School and Salk Institute for Biological Sciences. Nulliparous mice were littermate controls of mice profiled at pregnancy, lactation, or involution. For timed pregnancies, female B6 mice were set up at 6-8 wks of age with male B6 mice, female mice with plugs were separated and housed individually for the duration of pregnancy. Germ free mice and Kaede mice. Germ free (GF) B6 mice were purchased at the listed specific timepoints (nulliparous, gestation, lactation and involution at 6-8 weeks of age) from the University of California San Diego. GF mice were conventionalized by oral gavage of fecal microbiota from SPF B6 mice, one week prior to mating and maintained in SPF conditions. Kaede reporter mice were obtained from O. Kanagawa (RIKEN, Wako, Japan) and maintained on the B6 background. Kaede mice were mated at 6-8 weeks of age and collected at mid pregnancy (G14) and late pregnancy/lactation (G18/L1) followed the same age and experimental time points as the above mice. Thymectomized B6 mice were ordered from Jackson Labs, Jackson Labs thymectomized the mice at 4 weeks of age and we received them at 6 weeks and set up for mating at 7-8 weeks.

Wild animals

Study did not involve wild animals.

Reporting on sex

The findings of this study primarily apply to female mice, as we are specifically examining pregnancy-related changes, which are biologically unique to females. Therefore, the results are relevant only to female mice.

Field-collected samples

Study did not involve samples collected from the field.

Ethics oversight

All experiments were performed following guidelines listed in animal protocols (IS00001257, Harvard Medical School) and (23-00007, Salk Institute for Biological Studies) approved by the Institutional Animal Care and Use Committee.

Note that full information on the approval of the study protocol must also be provided in the manuscript.

Plants

Seed stocks

Report on the source of all seed stocks or other plant material used. If applicable, state the seed stock centre and catalogue number. If plant specimens were collected from the field, describe the collection location, date and sampling procedures.

Novel plant genotypes

Describe the methods by which all novel plant genotypes were produced. This includes those generated by transgenic approaches, gene editing, chemical/radiation-based mutagenesis and hybridization. For transgenic lines, describe the transformation method, the number of independent lines analyzed and the generation upon which experiments were performed. For gene-edited lines, describe the editor used, the endogenous sequence targeted for editing, the targeting guide RNA sequence (if applicable) and how the editor was applied.

Authentication

Describe any authentication procedures for each seed stock used or novel genotype generated. Describe any experiments used to assess the effect of a mutation and, where applicable, how potential secondary effects (e.g. second site T-DNA insertions, mosiacism, off-target gene editing) were examined.

Flow Cytometry

Plots

Confirm that:

☒ The axis labels state the marker and fluorochrome used (e.g. CD4-FITC).

☒ The axis scales are clearly visible. Include numbers along axes only for bottom left plot of group (a 'group' is an analysis of identical markers).

☒ All plots are contour plots with outliers or pseudocolor plots.

☒ A numerical value for number of cells or percentage (with statistics) is provided.

Methodology

Sample preparation

Mammary gland: Inguinal lymph nodes were removed and mammary glands 3, 4 and 5 were collected, minced and dissociated in collagenase solution (3mg/mL collagenase type II (Sigma C6885) and 2% FBS in DMEM) in a 37℃ shaking water bath for 20 min with manual shaking every 5 min, followed by red blood cell lysis. Single cell suspensions were filtered and

	washed with 2% DMEM solution. Thymus and LN: Lymphocytes from thymus and inguinal lymph nodes were obtained by mechanical disruption, filtered and washed with 10% RPMI solution. Intestines: Small and large intestinal tissues were measured, cleaned, and treated with RPMI containing 1mM DTT, 20mM EDTA and 2% FBS at 37℃ for 15 min to isolate the epithelial and IEL fractions. For the lamina propria (LP) fraction, the remaining tissue was dissociated in collagenase solution (1 mg/mL collagenase VIII (Sigma C2139), 50 g/ml DNase (Sigma C6885) in 1%FBS in RPMI) with constant stirring at 37℃ for 30min. Single cell suspensions for the IEL and LP fractions were filtered and washed with 10% RPMI solution. Spleen: Tissue was mechanically disrupted, followed by red blood cell lysis. Single cell suspensions were filtered and washed with 10% RPMI solution.
Instrument	Cells were acquired with a BD LSRII or BD FACSymphony A3.
Software	Flow cytometry analysis was performed with FlowJo 10 software.
Cell population abundance	The abundance and purity of cell populations in post-sort fractions were determined by re-analyzing the sorted sample using flow cytometry, to assess the percentage of target cells relative to the total cell population.
Gating strategy	The gating strategy involved FSC/SSC gates to select lymphocytes followed by live CD45, and TCRb gates. All the flow data reported here were always Live CD45+ TCRb+. A detailed gating strategy is included in supplementary information.

☒ Tick this box to confirm that a figure exemplifying the gating strategy is provided in the Supplementary Information.